HAL
open science

Variable structure dynamics in a bouncing dimer

Caishan Liu, Zhen Zhao, Bernard Brogliato

To cite this version:

Caishan Liu, Zhen Zhao, Bernard Brogliato. Variable structure dynamics in a bouncing dimer. [Research Report] RR-6718, INRIA. 2008. inria-00337482

HAL Id: inria-00337482

https://inria.hal.science/inria-00337482v1

Submitted on 7 Nov 2008

HAL is a multi-disciplinary open access archive for the deposit and dissemination of scientific research documents, whether they are published or not. The documents may come from teaching and research institutions in France or abroad, or from public or private research centers.

L'archive ouverte pluridisciplinaire **HAL**, est destinée au dépôt et à la diffusion de documents scientifiques de niveau recherche, publiés ou non, émanant des établissements d'enseignement et de recherche français ou étrangers, des laboratoires publics ou privés.

INSTITUT NATIONAL DE RECHERCHE EN INFORMATIQUE ET EN AUTOMATIQUE

Variable structure dynamics in a bouncing dimer

Caishan Liu and Zhen Zhao — Bernard Brogliato

N° 6718

November 2008

Thème NUM

Rapport de recherche

ISSN 0249-6399 ISRN INRIA/RR--6718--FR+ENG

INSTITUT NATIONAL DE RECHERCHE EN INFORMATIQUE ET EN AUTOMATIQUE
INRIA
centre de recherche GRENOBLE - RHÔNE-ALPES

Variable structure dynamics in a bouncing dimer

Caishan Liu and Zhen Zhao [*], Bernard Brogliato [†*]

Thème NUM — Systèmes numériques
Équipes-Projets Bipop

Rapport de recherche n° 6718 — November 2008 — 61 pages

Abstract: Systems with unilateral constraints usually possess a variable structure dynamics, in which systems can switch from one mode to another due to contacts and impacts. In particular, friction participating into contacts and impacts will extremely complicate the dynamics, and even result in some singularities when using rigid body models. In this paper, we develop a method that can well deal with the difficulties involved in the variable structure systems, such as the multiple impacts with friction (i.e. the occurrence of simultaneous impacts), the superstatic problems in rigid body systems, the multivalued graph in the stick mode of the Coulomb's friction, and the inelastic collapse in impacts. The transition rules to monitor the switches from one mode to another are also established, in which the normal states at each contact point are controlled by the complementary conditions for a contact process and by the potential energy at contact points for an impact process, while the tangential states at the contact point will be governed by a correlative coefficient of friction defined by the tangential differential equations. A system elaborated in [38] with precise experimental results serves as an example to illustrate the theoretical developments, in which a dimer consisting of two spheres rigidly connected by a light glass rod bounces on a vibrating plate. This system, even though simple enough, exhibits profuse physical phenomena under different initial and driving conditions, and may spur different ordered persistent motions, such as the drift, jump and flutter modes. In particular, each mode of the persistent motion is synthesized by a periodically complicated motion that may involve single and double impacts, contacts with or without slip, *etc.* Based on the theory proposed in this paper, we clearly explain the regime of persistent motions in the dimer and find that the peculiar property of friction with discontinuity plays a significant role for its formation. Plenty of numerical simulations are carried out, and precise agreements between the numerical and experimental results are obtained. Furthermore, a simplified model for the dimer in drift mode is developed and theoretical analysis is implemented. An approximate formula for the mean horizonal velocity is obtained that also coincides well with the experimental findings. This may be beneficial for the study

[*] State Key Laboratory for Turbulence and Complex Systems, College of Engineering, Peking University, Beijing, China, 100871
[†] INRIA, Bipop Research Team, ZIRST Montbonnot, 655 Avenue de l'Europe, F-38334 Saint-Ismier, France

Centre de recherche INRIA Grenoble – Rhône-Alpes
655, avenue de l'Europe, 38334 Montbonnot Saint Ismier
Téléphone : +33 4 76 61 52 00 — Télécopie +33 4 76 61 52 52

of complex systems dynamics, in which there exists an intrinsic connection between the ordered behaviors of the systems and the microsize parameters of its ingredients.

Key-words: nonsmooth mechanical system, impact, Coulomb friction, complex systems, numerical simulation.

Dynamique à structure variable d'un dimère rebondissant

Résumé : Les systèmes avec contraintes unilterales possèdent une structure variable, avec plusieurs modes définis par les onctacts avec ou sans frottement et les impacts. Dans cet article nous proposons une mt́hode num'erique associée à un modèle d'impacts multiples avec frottement, afin de simuler un dimère qui rebondit sur une table vibrante. Un tel système, bien que relativement simple, incorpore la plupart des difficultés liées au caractère non-régulier des systèmes avec contact unilatéral frotant. Les résultats numériques sont comparés avec succès aux résultats expérimentaux présentés par Dorbolo et al. (Physical Review Letters, 95, 2005).

Mots-clés : mécanique non-régulière, impacts, frottement de Coulomb, simulation numérique, systèmes complexes.

1 Introduction

Multibody systems with nonsmooth interface laws (unilateral constraints, friction, etc) are ubiquitous in many fields of application (aerospace, automotive systems , granular matter, circuit breakers industry, nuclear plants, bipedal locomotion, robotics, biological engineering, etc), and have been attracting the attention of researchers in many fields including multibody dynamics [1], systems and control [3], applied mathematics [4], mechanical engineering [2], particle physics [5], biology [6], *etc*. The challenges from such systems are to provide accurate and realistic responses for systems with discontinuous events, and to establish a uniform theoretical framework to describe the complex behavior. The first issue is related to the problem of modeling contacts/impacts with or without friction in rigid body systems. The second one is associated with the description of complex systems, in which the physical mechanism of some ordered phenomena under certain actions of discrete events (like the swarming and swirling motion in granular matter) are still ambiguous [7, 8, 9].

The feature of multibody systems with unilateral constraints and friction is that their structure is time-varying, since the contact points status may change from active to inactive, stick to slip, *etc*. Obviously, more contact points will make the topology of these systems more complex and even singular in certain dynamical situations. For instance, superstatic problems may be met when the number of the active contacts is larger than the number of degrees of freedom [10]. The Painlevé paradox can be induced by the combination of Coulomb's friction with certain special configurations of the system [11, 12, 13, 53], multiple impacts (i.e. several collisions occurring at the same time on the system) with or without friction may occur [2, 14]. The classical restitution laws cannot provide unique and consistent solutions for the velocity outcomes of such nonsmooth systems [15, 16], and the peculiar property of dry friction will generate plenty of singularities in the rigid body models [54, 55]. Moreover, the transition rules to monitor the switches from one mode to another are still unclear and lack of proper description, such as the transition from stick to slip or its reversal motions, and the problem of inelastic collapses in which a sequence of impacts will converge to a contact phase [57]. Therefore, solving multibody systems with unilateral constraints within the framework of rigid body dynamics requires deep modeling and analysis in various aspects of scientific activities: applied mathematics, mechanics and physics. An overview on the subject can be found in [17, 10, 18].

From the mathematical point of view, the Coulomb's friction law and the unilateral constraints lend themselves to representations with Linear or Nonlinear Complementary Problems (LCP or NCP) [18, 2, 4]. Compact formulations using LCP or NCP tools allow one to describe the dynamics of variable structure systems within a uniform framework. However, the essential features of the nonsmooth interface laws, like the multivalued graph of Coulomb's law at zero tangential velocity and the discontinuity of impacts, will generate tiny structures in both the contact and impact processes. In particular, these tiny structures usually play a significant role for the global behavior of the systems, and need to be carefully checked in order to efficiently monitor the transitions between various contact/impact status. Therefore, the improvements of the mathematical theories related to the variable structure dynamics require further investigations on the aspect of physical modeling, especially in dealing with the events of multiple contacts/impacts with friction, and the singularities appearing in rigid body models.

Multiple impacts have a crucial influence on the long-term dynamics of a system with variable structures and may spur some ordered phenomena, such as the so-called

solitary wave in 1D chain systems [19, 20, 21, 22, 23, 24, 25, 26, 27, 28, 29, 30, 31], different pattern formation in vibrated layers [5], the *swarming and swirling* states in self-propelled rods [8, 32, 34, 35, 33, 36, 37], *etc*. From the energetic point of view, two main effects will be involved in the complex phenomena of multiple impacts: local effects at the contact points (that imply energy dissipation through plastic deformation and friction as well as other dissipation forces), and global effects that affect the whole system and take the form of waves traveling through the system (the global effects are responsible for the *energy dispersion* among the various bodies in the system) [30]. At present, there exists various models to take account of the interactions between contact bodies: some of them based on restitution mappings (like the Newton's or Poisson's coefficient) [38, 39, 40]. The principal drawbacks of these models when dealing with multiple impacts (even frictionless) or single impacts with Coulomb friction, is that they are not able to separate the dissipation and the dispersion (wave or the couplings) effects, and there may be an infinite choice of coefficients for the same energetical behavior [3], so that the mechanical meaning of the coefficients is unclear. Hence these models may generate quite inaccurate numerical results. Alternative methods associated with force/compliance models will spur a process of multiscale calculation both in time and space levels, where the detailed information related to the very small deformation at local regions of bodies varying in a very short time should be investigated carefully. Obviously these methods also possess their own drawbacks, like the difficulty of estimating contact parameters and the stiff ODEs problems in numerical implementation, thus generating unpredictable results for simulations [41, 25, 42]. Therefore, the challenge in dealing with multiple impacts depends not only on the choice between rigid body or compliant models, but also on the level of numerical implementation when multiple scales occur.

Undoubtedly, the processes of multiple contacts and/or impacts will be further complicated by the frictional effects, in which different types of tangential motions (such as stick-slip, rolling without slip) may appear in the course of contacts and the short-time collisions. In particular, the multivalued part of Coulomb's graph that corresponds to the stick mode is much tough in using rigid body models. Some researchers argued that the Coulomb's model should be regularized at zero tangential velocity [42, 43] by smoothing the relationship between the normal and tangential forces over a small range of tangential velocity. However, this modification destroys the intrinsic properties of dry friction observed from amount of experiments, and renders some numerical results unpractical. In fact, the transition of the frictional modes from stick to slip or its reverse correspond to a global reflection for the complex behaviors in contacts with friction, and depends not only on the material properties of the contact bodies but also on the dynamics of the systems. The physical phenomena like the sudden collapses of steady states [33] and the ordered behaviors in elongated particles [34, 35] imply that the multivalued part of the Coulomb's law has to be kept in the analysis and is significant for the numerical simulation [45, 46]. Nevertheless, the dependence of frictional forces on the normal contact forces will bring many difficulties in monitoring the discontinuity of the tangential motion, and also in the calculations for the contact forces in the stick mode due to the multivalued property of the Coulomb's graph. In this paper, a *correlative coefficient of friction* depending on the dynamical equations in stick mode is introduced, and the difficulties mentioned above can be well overcome.

The goal of this paper is to propose a method for dealing with the dynamics of variable structure systems. The addition and deletion of constraints as well as the events of impacts are anticipated to be solvable. In particular, the event of multiple impacts with friction that usually play a significant role on the global behavior of systems will

be emphasized in this paper. According to a preliminary work for frictionless multiple impacts [47, 48], the so-called Darboux-Keller approach [49, 16, 45, 3] will be extended to the case of frictional multiple impacts. In this method the local energy loss is confined by Stronge's energetic coefficient [15, 50], while the dispersion effects are reflected by a distributing law that is related to the relative stiffness and the mode of the potential energy accumulation between contacting bodies [47]. In the absence of friction, the comparisons between our numerical predictions and the experimental results found in the literature [21] show very good agreements [30, 48], thus validating the proposed algorithm and model. When friction participates into multiple impacts, the tiny structures of the impulsive dynamics induced by the Coulomb's friction will be carefully investigated, and then combine with the method in [47, 48] to make the frictional multiple impacts solvable.

The development of the method proposed in this paper for the variable structure dynamics will be illustrated by using a simple system experimentally investigated in [38]. The simple system, a dimer, consists of two spheres rigidly connected by a light rod that bounces on a vibrating plate. Under different initial and driving conditions, the vibrated dimer can be excited with various modes of persistent motion, including the Flutter (F) mode in which the tips of the dimer hit the plate out of the phase at every other period of collision, the Jump (J) mode in which both tips collide with the plate once every cycle of the vibration of the plate, and the Drift (D) mode in which a persistent horizontal drift is observed. In particular, the experiments show that the drift of the dimer is a concatenation of multiple collisions that include individual, double, and rolling contacts. Obviously, the dimer, though simple enough, encapsulates most difficulties of nonsmooth mechanical systems such as the superstatic problem in rigid body model, the discontinuity of tangential motion due to friction, the single and multiple impacts with friction. Moreover, one can anticipate that the mechanism exhibited in the simple system would benefit to the studies of collective dynamics in complex systems of self-propelled (SP) particles [7, 8, 34, 35, 51]. Therefore, the dynamics of a bouncing dimer plays a significant role both in nonsmooth systems and granular matter.

The paper is organized as follows: Section 2 describes the dimer model and presents the governing equations that will vary with the contact status of the tips. The topology of the contact states in the dimer will be presented in Section 3, in which a correlative coefficient of friction is introduced to identify the transition from stick to slip or its reverse. The singularity of the superstatic problem that may appear in the dimer with contact phases is also discussed in this section. The impulsive differential equations based on the Darboux-Keller's method are established in section 4, in which the distributing law proposed in [47] for multiple impacts will be briefly introduced, and the tiny structures induced by the Coulomb's friction in impacts will be discussed in detail. The problem of inelastic collapse that is associated with a transition from a sequence of impacts to a contact phase will also be illustrated in this section, and a guideline for the identification of the transition is presented. In section 5, we analyze the experimental phenomena presented in [38], and combine the correlative coefficient of friction with the experimental specifics to estimate the practical value of the static coefficient of friction that will be applied into the numerical simulations. The comparison between numerical and experimental results is carried out in section 6, and the difference for the slip coefficient of friction between impacts and contacts is claimed. Moreover, the influence of the initial and driving conditions on the formation of the persistent motions in the dimer is also investigated. According to the numerical observations, a simplified model for the dimer in a drift mode is presented in section 7, and

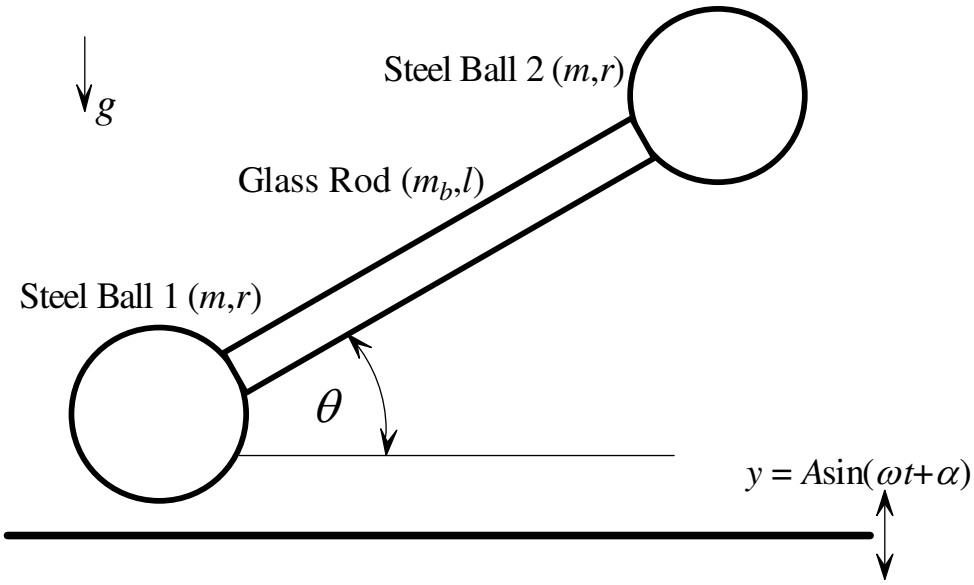

Figure 1: A dimer bouncing on a vibrated plate.

an approximate formula for the mean speed of the drift motion is obtained that can well reflect the connection between the global drift motion and the micro parameters in the dimer. Summaries and conclusions are given in the final section 8.

2 The dynamics of a bouncing dimer

Fig.1 depicts for the dimer experimentally studied in [38], in which two steel spheres are rigidly connected by a light glass rod with 4mm diameter, and placed on a plate that vibrates with a sinusoidal waveform. Let us denote (m_b, r) the mass of the sphere and its radius, respectively. The mass of the rod is m_r and its length is $(l - 2r)$ that is varied to change the aspect ratio $A_r = (1 + 0.5l/r)$ [38]. In the laboratory frame of reference the oscillation of the plate is

$$y_p(t) = A\cos(\omega t + \alpha) \tag{1}$$

with amplitude A and frequency f, and α is the initial phase angle of the plate oscillation related to the reference time for simulation. Let us denote (x_1, y_1), (x_2, y_2) and (x_r, y_r) the coordinates of the mass centers of the left ball, right ball and the glass rod, respectively. The tilt angle of the rod is denoted as θ. With these kinematical quantities, the kinetic energy of the dimer in motion can be expressed as

$$T = \frac{1}{2}m_b(\dot{x}_1^2 + \dot{y}_1^2 + \dot{x}_2^2 + \dot{y}_1^2) + \frac{1}{2}m_r(\dot{x}_r^2 + \dot{y}_r^2) + \frac{1}{2}(2J_b + J_r)\dot{\theta}^2 \tag{2}$$

where $J_b = 2m_b r^2/5$, $J_r = m_r(l - 2r)^2/12$ are the inertias of the ball and the rod with respect to their mass centers, respectively. The positions between the mass centers of the left and right balls as well as the glass rod can be connected by the following

geometrical relationships:

$$x_2 = x_1 + l\cos\theta,\ y_2 = y_1 + l\sin\theta \tag{3}$$
$$x_r = x_1 + 0.5l\cos\theta,\ y_r = y_1 + 0.5l\sin\theta.$$

Let us introduce the so-called *local* coordinates, following an established terminology [18]. We consider the two points (one for each ball) that are the closest to the plate. Their normal coordinates in the fixed frame are

$$x_{n_1} = y_1 - r, \quad x_{n_2} = y_2 - r = y_1 + l\sin\theta - r \tag{4}$$

The local tangential relative positions, that correspond to the local sliding velocities, are given by:

$$x_{\tau_1} = x_1 + r\theta, \quad x_{\tau_2} = x_2 + r\theta = x_1 + l\cos\theta + r\theta \tag{5}$$

Let us select $\mathbf{q} = [x_1, y_1, \theta]^T \in \mathbb{R}^3$ as the generalized coordinates of the system, and define $\mathbf{X}_c = [x_{n_1}, x_{n_2}, x_{\tau_1}, x_{\tau_2}]^{\mathbf{T}} \in \mathbb{R}^4$. The vector for the contact forces at the tips is denoted as $\mathbf{F} = [F_{n_1}, F_{n_2}, F_{\tau_1}, F_{\tau_2}]^{\mathbf{T}} \in \mathbb{R}^4$. It is noteworthy that F_{τ_i} and F_{n_i} equal zero when the $i-$th contact ($i = 1, or, 2$) is not closed. The Euler-Lagrange equations of the dimer are (the time argument is dropped):

$$\mathbf{M}(\theta)\ddot{\mathbf{q}} - \mathbf{h}(\theta, \dot{\theta}) = \mathbf{K}^{\mathbf{T}}(\theta)\mathbf{F} + \mathbf{Q}_g(\theta) \tag{6}$$

where $\mathbf{M}(\theta)$ is a 3×3 mass matrix,

$$\mathbf{M}(\theta) = \begin{bmatrix} 2m_b + m_r & 0 & -l\sin\theta\,(m_b + 0.5m_r) \\ 0 & 2m_b + m_r & l\cos\theta\,(m_b + 0.5m_r) \\ -l\sin\theta(m_b + 0.5m_r) & l\cos\theta\,(m_b + 0.5m_r) & (m_b l^2 + 0.25m_r l^2 + 2J_b + J_r) \end{bmatrix} \tag{7}$$

and $\mathbf{h}(\theta, \dot{\theta})$ and $\mathbf{Q}_g(\theta)$ are the vectors of the inertial forces and the generalized forces due to gravity, respectively:

$$\mathbf{h}(\theta, \dot{\theta}) = \left[\dot{\theta}^2 l\cos\theta\,(m_b + 0.5m_r), \dot{\theta}^2 l\sin\theta\,(m_b + 0.5m_r), 0\right]^T$$
$$\mathbf{Q}_g(\theta) = g\,[0, -(2m_b + m_r), -(m_b + 0.5m_r)l\cos\theta]^T \tag{8}$$

The matrix $\mathbf{K}^T(\theta)$ is the Jacobian matrix,

$$\mathbf{K}^T(\theta) = \begin{bmatrix} 0 & 0 & 1 & 1 \\ 1 & 1 & 0 & 0 \\ 0 & l\cos\theta & r & r - l\sin\theta \end{bmatrix} \tag{9}$$

The matrix $\mathbf{K}(\theta)$ also connects the two potential contact points cartesian velocities and accelerations with the generalized velocity $\dot{\mathbf{q}}$ and generalized accelerations $\ddot{\mathbf{q}}$,

$$\dot{\mathbf{X}}_c = \mathbf{K}(\theta)\dot{\mathbf{q}} \tag{10}$$

and

$$\ddot{\mathbf{X}}_c = \mathbf{K}(\theta)\ddot{\mathbf{q}} + \mathbf{S}(\theta, \dot{\theta}) \tag{11}$$

where

$$\mathbf{S} = \left[0, -l\dot{\theta}^2 \sin\theta, 0, -l\dot{\theta}^2 \cos\theta\right]^T . \tag{12}$$

The solution of (6) depends on the contact forces acting at the two potential contact points, which are closely associated with the contact status at the tips of the left and right balls in the dimer (the points directly underneath the geometric center of the balls during the motion of the dimer). In order to detect the contact status and to determine the contact forces at both tips, the local dynamical equations are established by combining (6) with (11) (next we drop the argument θ),

$$\ddot{\mathbf{X}}_c = \mathbf{KM^{-1}K^T F} + \mathbf{KM^{-1}(h + Q_g)} + \mathbf{S} \tag{13}$$

From Eq.13, the normal and tangential accelerations can be separately expressed as

$$\ddot{\mathbf{x}}_n = \mathbf{AF}_n + \mathbf{BF}_\tau + \mathbf{H}_n \tag{14}$$

and

$$\ddot{\mathbf{x}}_\tau = \mathbf{CF}_n + \mathbf{DF}_\tau + \mathbf{H}_\tau \tag{15}$$

where $\ddot{\mathbf{x}}_n = [\ddot{x}_{n_1}, \ddot{x}_{n_2}]^T$, $\ddot{\mathbf{x}}_\tau = [\ddot{x}_{\tau_1}, \ddot{x}_{\tau_2}]^T$, $\mathbf{F}_n = [F_{n_1}, F_{n_2}]^T$, $\mathbf{F}_\tau = [F_{\tau_1}, F_{\tau_2}]^T$, $\mathbf{KM^{-1}K^T} = \begin{pmatrix} A & B \\ C & D \end{pmatrix}$. $\mathbf{H}_n = [H_{n_1}, H_{n_2}]^T$ and $\mathbf{H}_\tau = [H_{\tau_1}, H_{\tau_2}]^T$ are the terms of the normal and tangential accelerations induced by the applied and inertial forces.

The status of each contact point will be analyzed according to Eq.14 and 15, and then provide the proper constraint equations to make Eq.6 solvable.

3 The topology of the contact states

There are three qualitatively different regimes for the contact status at each tip of the left and right balls: *free motion* in which the contact at the tip is not closed; *continuous slide* in which the sphere at the tip is rolling with slip on the oscillated plate; *stick mode* in which the corresponding sphere will purely rotate without slip. The contact status at each tip will determine the dynamical behavior of the dimer during a long-term contact dynamics or a short-term collision process. The impact dynamics of the dimer will be discussed in section 4. In this section, we will investigate the topology of the dimer dynamics in the contact phases.

The system modes of the dimer are the combinations of the contact status at each tip of the left and right spheres. Theoretically speaking, for the dimer there are 3^2 different kinds of modes. By considering the symmetry of the contact status at the tips of the left and right balls, we can classify the modes of the dimer as: the *free mode* in which the dimer is airborne; the *single-slip mode* in which one tip is in contact with the plate with *continuous slide*, while the other tip wis in *free motion*; the *single-stick mode* in which one tip purely rolls without slip on the plate, while the other is airborne; *double-slip mode* in which both tips with *continuous slide* are in contact with the plate; and *double-stick mode* in which both tips take the stick mode. The system state of one tip with *continuous slide* and the other with *stick mode* cannot appear due to the assumption of perfect rigidity, hence there are 7 modes.

The modes are influenced by the unilateral constraints and the friction effects between the plate and the dimer. Therefore the rules for the transitions between different contact status should be established. They depend on the properties of the normal and tangential constraints applied by the contacts with friction.

3.1 The complementary condition in the normal direction

The *free motion* mode can be easily identified by using the following gap functions for the relative displacements between the tips and the plate,

$$\delta_i = x_{n_i} - y_p(t), \quad (i = 1, 2) \tag{16}$$

with the following complementarity conditions in the normal direction at each unilateral constraint,

$$\delta_i \cdot F_{n_i} = 0,\ \delta_i \geq 0,\ F_{n_i} \geq 0, i = 1, 2. \tag{17}$$

However, things complicate when one or two contact points persist on the oscillated plate because there may be transitions between various contact status. For instance, the tip may change from rolling to sliding, or slip reversal, or detachment. If at time t

$$\delta_i(t) = 0, \dot{\delta}_i(t) < 0, \quad (i = 1, 2), \tag{18}$$

an event of impacts is triggered at the tip i, and impulsive equations for the dimer should be established to obtain the velocities outcomes after the discrete event. This case will be discussed in section 4.

When $\delta_i = \dot{\delta}_i = 0$, the contact at tip i is closed and one has to rewrite the complementarity conditions at the acceleration level in order to detect the transition between various contact modes [44],

$$\ddot{\delta}_i \cdot F_{n_i} = 0,\ \ddot{\delta}_i \geq 0,\ F_{n_i} \geq 0, i = 1, 2. \tag{19}$$

We may rewrite (19) more compactly as

$$0 \leq \mathbf{F}_n \perp \mathbf{A}\mathbf{F}_n + \mathbf{B}\mathbf{F}_\tau + \mathbf{H}_n - \begin{pmatrix} \ddot{y}_p(t) \\ \ddot{y}_p(t) \end{pmatrix} \geq 0 \tag{20}$$

As we shall see, solving this set of complementarity conditions whose unknown is $\mathbf{F}_n$ requires some analysis (in particular (15) and the friction law will play a role).

3.2 Coulomb's friction

When friction is present at the contacts, the relative tangential motion and the contact forces will be mutually influenced. Usually, the peculiar property of dry friction is described by the following Coulomb's law. In the *continuous slide mode* for the tip i, the normal and tangential contact forces should satisfy the following linear relationship,

$$F_{\tau_i} = -\mu_i F_{n_i} sign\left(\frac{\mathbf{v}_{\tau_i}}{|\ \mathbf{v}_{\tau_i}\ |}\right), \text{ if } \mathbf{v}_{\tau_i} \neq 0, i = 1, 2, \tag{21}$$

where $\mathbf{v}_{\tau_i}$ is the relative tangential velocity, and $\mathbf{v}_{\tau_i} = \dot{x}_{\tau_i}$, $(i = 1, 2)$. $\mu_i > 0$ is the slip friction coefficient at the tip i.

Once the event of $\mathbf{v}_{\tau_i} = 0$ is detected, the contact status at tip i cannot be uniquely determined since the tip may stick or continuously slip with a reversal direction on the plate. Considering the fact that the Coulomb friction law represents a constraint at the force level, the contact status of the *stick mode* at tip i should be defined at the acceleration level [10, 44], thus a new constraint except for $\mathbf{v}_{\tau_i} = 0$ should be added into the *stick mode*.

$$| F_{\tau_i} | \leq \mu_{s_i} F_{n_i}, \text{ if } \mathbf{v}_{\tau_i} = 0 \text{ and } \dot{\mathbf{v}}_{\tau_i} = 0, \tag{22}$$

where $\mu_{s_i} > \mu_i$ is the static coefficient of friction. If $\dot{\mathbf{v}}_{\tau_i} \neq 0$ at the instant of $\mathbf{v}_{\tau_i} = 0$, the relative tangential motion at the contact point i will not stop but take a reversal slip when the relative tangential velocity $\mathbf{v}_{\tau_i}$ passes through zero. In this case, the contact force at tip i is still kept on the surface of the friction cone, and there exists a linear relationship between the normal and tangential force that satisfies the Coulomb's law for slip. A problem arising in this situation is how to determine the future slip direction. In the planar cases, the slip will be reversal and the direction of the friction force can be easily determined. For the spatial cases, the future slip direction has to coincide with the one of the relative tangential acceleration $\dot{\mathbf{v}}_{\tau_i}$ at the instant of $\mathbf{v}_{\tau_i} = 0$ [45]. Therefore, the Coulomb's friction law in this situation is modified to:

$$F_{\tau_i} = -\mu_i F_{n_i} sign\left(\frac{\dot{\mathbf{v}}_{\tau_i}}{| \dot{\mathbf{v}}_{\tau_i} |}\right), \text{ if } \mathbf{v}_{\tau_i} = 0 \text{ and } \dot{\mathbf{v}}_{\tau_i} \neq 0, i = 1, 2. \tag{23}$$

3.3 Transition between various system states

The transition from contact to detachment will be governed by the complementarity conditions in the normal direction at the contact points, while the one from slip to stick is determined by the Coulomb's law. In particular, the coupling between the normal and tangential motions at contact points significantly complicates the transition between various system's modes. Because the contact status of each contact point in the normal and tangential directions are governed by different constraint equations, the identification for the transition of the contact status should be separately carried out in the normal and tangential directions at each contact point.

Let us first consider the simplest case in which the dimer is assigned with a *single slip mode* at the tip i in contact with the plate. So we have $\delta_i = 0$, $\dot{\delta}_i = 0$, $\dot{x}_{\tau_i} \neq 0$, and $F_{n_j} = F_{\tau_j} = 0$, $(j \neq i)$. From Eq.14, the normal accelerations can be expressed as:

$$\ddot{x}_{n_i} = A_i F_{n_i} + B_i F_{\tau_i} + H_{n_i} \tag{24}$$

where A_i and B_i are the (i, i)th elements of the matrices $\mathbf{A}$ and $\mathbf{B}$ in Eq.14, respectively. The tangential relative acceleration at the tip i is

$$\ddot{x}_{\tau_i} = C_i F_{n_i} + D_i F_{\tau_i} + H_{\tau_i} \tag{25}$$

where C_i and D_i are the (i, i)th elements of the matrices $\mathbf{C}$ and $\mathbf{D}$ in Eq.15, respectively. If the single slip mode is kept at tip i at time t, i.e. $\dot{x}_{\tau_i}(t) \neq 0$, then the tangential constraint at this instant is:

$$F_{\tau_i} = -\mu_i F_{n_i} sign(\dot{x}_{\tau_i}(t_k)) \tag{26}$$

The combination of (24) and (26) leads to

$$\ddot{x}_{n_i} = \hat{A}_i F_{n_i} + H_{n_i} \tag{27}$$

where $\hat{A}_i = A_i - \mu_i B_i sign(\dot{x}_{\tau_i}(t_k))$. It is clear that Eq.27 is an algebraic equation only related to the variables $\ddot{x}_{n_i}$ and F_{n_i}, which should satisfy the complementarity condition as expressed in Eq.19. If $\hat{A}_i > 0$, the normal contact force F_{n_i} can be uniquely

determined according to the complementarity condition, and thus the tangential force F_{τ_i} can also be obtained based on Eq.26. The values of F_{n_i} and F_{τ_i} are the constraint forces produced by tip i at the instant t_k. Then, the simulation for the dynamical equation (6) can be advanced based on the states $(\mathbf{q}_k, \dot{\mathbf{q}}_k)$ at time t_k. If the solution from the complementarity condition is $F_{n_i} = 0$ and if $\ddot{x}_{n_i} > 0$, this implies that a detachment occurs at this instant, and a free mode is generated for the dimer.

In some special configurations, the value of $\hat{A}_i$ may be less than zero. This is related to Painlevé paradoxes that may arise in rigid body dynamics (there exists multiple solutions or even no solution at all for Eq.27). Detailed discussion on this problem can be found in [3, 11, 12, 13, 52, 53]. For the case of no solution in Painlevé paradoxes, a tangential impact will appear at the contact point according to the experimental validation for a two-link robotic system [11, 12]. Thus, the impulsive dynamics described in the next section can be used if the paradoxical situations occur.

If $\dot{x}_{\tau_i}(t) = 0$ is checked, the transition of the contact status in the tangential direction may occur due to the peculiar property of the Coulomb's friction. However, the difficulty arising in this case is that the property of the friction is not known previously, such that we cannot confirm which constraint equations from the Coulomb's law should be applied on the tangential direction of the contact point. An iterative method for searching the proper tangential constraint is necessary. Let us first set $\ddot{x}_{\tau_i}(t_k) = 0$ for Eq.15. Then, we can obtain a relationship between the normal and tangential forces for the stick mode,

$$F_{\tau_i} = -\frac{1}{D_i}[C_i F_{n_i} + H_{\tau_i}] \tag{28}$$

Substituting Eq.28 into Eq.24 leads to a new algebraic equation for the normal force F_{n_i} and the normal acceleration $\ddot{x}_{n_i}$,

$$\ddot{x}_{n_i} = [A_i - \frac{C_i}{D_i}]F_{n_i} + H_{n_i} - \frac{H_{\tau_i}}{D_i} \tag{29}$$

Thus Eq.29 is an algebraic equation for the contact status with a tangential stick mode, and then the complementarity condition (19) can be used to obtain the normal contact force F_{n_i}. After that, the tangential force F_{τ_i} in the stick mode can be easily calculated by Eq.28. It is noteworthy that the values of F_{n_i} and F_{τ_i} are true only if the system is in the stick mode. Therefore, we should recheck the condition for the occurrence of the stick mode. Let us define a coefficient termed as the *correlative coefficient of friction*, as

$$\mu_{st}^i = \frac{|F_{\tau_i}|}{F_{n_i}} \tag{30}$$

A transition from slip to stick will appear at the instant t_k only if $\mu_{st}^i < \mu_{s_i}$, and then the normal and tangential forces F_{n_i} and F_{τ_i} obtained from the stick mode can be applied into Eq.6 to advance the simulation.

If $\mu_{st}^i > \mu_{s_i}$, the tangential constraint should be replaced by the Coulomb's friction for slip since the contact force is not located in the interior of the friction cone at the instant of t. However, the direction of the possible tangential velocity is also unknown at the instant of $\dot{x}_{\tau_i}(t) = 0$, since the sign assigned on the friction force cannot be known in advance. These problems are discussed in [54, 55, 56, 45, 46], in which theoretical results and numerical schemes are developed. By combining the tangential constraint for slip with the normal motion expressed in Eq.24, it is clear that the contact forces can be obtained by using the complementarity conditions at the contact point.

Transition from stick to slip may appear in the case of the dimer with a *single stick mode*, which can also be monitored by using the *correlative coefficient of friction* obtained from the stick mode. If $\mu_{st}^{i} < \mu_{s_i}$, the stick mode will be preserved at the instant t. Otherwise, the contact point i will resume to slip since the friction cone has been shaken off.

When more contact points are closed, the calculation for the contact forces and the transition between various system states will be more complex. Let us consider the situation of the dimer with a *double-slip mode* at time t, in which $\delta_i(t) = 0$, $\dot{\delta}_i(t) = 0$, $\dot{x}_{\tau_i}(t) \neq 0, (i = 1, 2)$. By using the tangential constraints for slip and Eq.14, we can obtain

$$\begin{bmatrix} \ddot{\mathbf{x}}_{n_1} \\ \ddot{\mathbf{x}}_{n_2} \end{bmatrix} = \hat{\mathbf{A}} \begin{bmatrix} F_{n_1} \\ F_{n_2} \end{bmatrix} + \begin{bmatrix} H_{n_1} \\ H_{n_2} \end{bmatrix} \tag{31}$$

where

$$\hat{\mathbf{A}} = \begin{bmatrix} A_{11} - \mu_1 B_{11} sgn(\dot{x}_{\tau_1}) & A_{12} - \mu_2 B_{12} sgn(\dot{x}_{\tau_2}) \\ A_{21} - \mu_1 B_{21} sgn(\dot{x}_{\tau_1}) & A_{22} - \mu_2 B_{22} sgn(\dot{x}_{\tau_2}) \end{bmatrix} \tag{32}$$

If $\hat{\mathbf{A}}$ is positive definite, the LCP in Eq.20 has a unique solution $\mathbf{F}_n$ and reads as $0 \leq \mathbf{F}_n \perp \hat{\mathbf{A}}\mathbf{F}_n + \mathbf{H}_n - \begin{pmatrix} \ddot{y}_p(t) \\ \ddot{y}_p(t) \end{pmatrix} \geq 0$. If $\hat{\mathbf{A}}$ is not positive definite, the so-called Painlevé paradox may appear. However this singularity does not occur along the simulated trajectories in this study.

Although the transition from a double stick to a single stick modes is impossible in the dimer system, a general discussion is presented in the following. Let us assume $\dot{x}_{\tau_1}(t) = 0$ while $\dot{x}_{\tau_2}(t) \neq 0$ at t. Thus, the tangential constraint at contact point 1 may be changed due to the occurrence of $\dot{x}_{\tau_1}(t) = 0$. From Eq.15, we can separate an equation for the tangential acceleration $\ddot{x}_{\tau_1}$,

$$\ddot{x}_{\tau_1} = C_{11} F_{n_1} + C_{12} F_{n_2} + D_{11} F_{\tau_1} - \mu_2 D_{12} sgn(\dot{x}_{\tau_2}) F_{n_2} + H_{\tau_1} \tag{33}$$

By setting $\ddot{x}_{\tau_1} = 0$, we can obtain

$$F_{\tau_1} = -\frac{1}{D_{11}} [C_{11} F_{n_1} + (C_{12} - \mu_2 D_{12} sgn(\dot{x}_{\tau_2})) F_{n_2} + H_{\tau_1}] \tag{34}$$

Thus, we have

$$\begin{bmatrix} \ddot{\mathbf{x}}_{n_1} \\ \ddot{\mathbf{x}}_{n_2} \end{bmatrix} = \hat{\mathbf{A}} \begin{bmatrix} F_{n_1} \\ F_{n_2} \end{bmatrix} + \begin{bmatrix} \hat{H}_{n_1} \\ \hat{H}_{n_2} \end{bmatrix} \tag{35}$$

Similarly to the previous cases, Eq.35 consists of a set of algebraic equations for the normal accelerations and normal forces that can be solved by using the normal complementarity conditions in Eq.20. The matrix $\hat{\mathbf{A}}$ should be positive definite so that there are no paradoxical situations. Then, the property of the tangential constraint can be identified from the correlative coefficient of friction. If

$$\mu_{st}^{1} = \frac{|F_{\tau_1}(t_k)|}{F_{n_1}(t_k)} < \mu_{s_1}, \tag{36}$$

a transition from slip to stick will appear at the contact point 1. Otherwise, if

$$\mu_{st}^{1} = \frac{|F_{\tau_1}(t_k)|}{F_{n_1}(t_k)} > \mu_{s_1}, \tag{37}$$

the tangential constraint should satisfy the Coulomb's friction law for slip, and values for all the contact forces at the two contact points should be recalculated.

For the dimer, it is possible that both $\dot{x}_{\tau_1}$ and $\dot{x}_{\tau_2}$ vanish simultaneously at a certain time t_k. In order to identify the properties of the tangential constraints at both contact points, we set $\ddot{x}_{\tau_1} = 0$ and $\ddot{x}_{\tau_2} = 0$ in Eq.15. If $\mathbf{D}$ is a full-rank matrix, the relationship between the tangential and normal forces can be expressed as

$$\mathbf{F}_\tau = -\mathbf{D}^{-1}\mathbf{C}\mathbf{F}_n - \mathbf{D}^{-1}\mathbf{H}_\tau \tag{38}$$

thus, we have

$$\ddot{\mathbf{x}}_n = \hat{\mathbf{A}}\mathbf{F}_n + \hat{\mathbf{H}}_n \tag{39}$$

where $\hat{\mathbf{A}} = \mathbf{A} - \mathbf{B}\mathbf{D}^{-1}\mathbf{C}$, $\hat{\mathbf{H}}_n = \mathbf{H}_n - \mathbf{B}\mathbf{D}^{-1}\mathbf{H}_\tau$. If $\hat{\mathbf{A}}$ is positive definite, the correlative coefficient of friction for each contact point can be deduced as:

$$\mu_{st}^1 = \frac{|F_{\tau_1}(t_k)|}{F_{n_1}(t_k)}, \quad \mu_{st}^2 = \frac{|F_{\tau_2}(t_k)|}{F_{n_2}(t_k)} \tag{40}$$

Obviously, there exist four different combinations between the values of the correlative coefficients of friction. If

$$\mu_{st}^1 < \mu_{s_1}, \quad \text{and} \;\; \mu_{st}^2 < \mu_{s_2}, \tag{41}$$

there will be a transition from a double-slip to double-stick modes. If one of the above conditions is violated, the tangential constraint corresponding to that one should be changed, and the contact forces should be recalculated until the tangential constraints applied beforehand are consistent with the contact forces obtained from the LCP's equations.

In summary, once the relative tangential velocity at a tip equals zero, a transition between the contact status may be triggered in the system. The property of the tangential constraints at this instant can be identified by a correlative coefficient of friction μ_{st}, which also represents a relationship between the normal and tangential forces for the contact point with a stick status. Thus the difficulty of the Coulomb's law with a multivalued graph can be overcome. In other words, the contact force that lies in the interior of the friction cone can be determined by using a correlative coefficient of friction μ_{st}.

3.4 The singularity in contact phases

As noted in above, some singularities, like the Painlevé paradox and the superstatic problems, may appear in the formulation. An obvious situation for this corresponds to the case when the dimer lies on the oscillated plate in which a superstatic problem may be spurred. Let us set $\theta = 0$, Eq.14 and Eq.15 can be written as

$$\begin{bmatrix} \ddot{x}_{n_1} \\ \ddot{x}_{n_2} \end{bmatrix} = \frac{1}{\beta}\begin{bmatrix} \beta_2 & \beta_3 \\ \beta_3 & \beta_2 \end{bmatrix}\begin{bmatrix} F_{n_1} \\ F_{n_2} \end{bmatrix} + \frac{1}{\beta}\begin{bmatrix} -rl & -rl \\ rl & rl \end{bmatrix}\begin{bmatrix} F_{\tau_1} \\ F_{\tau_2} \end{bmatrix} + \begin{bmatrix} -g \\ -g \end{bmatrix} \tag{42}$$

and

$$\begin{bmatrix} \ddot{x}_{\tau_1} \\ \ddot{x}_{\tau_2} \end{bmatrix} = \frac{1}{\beta}\begin{bmatrix} -rl & rl \\ -rl & rl \end{bmatrix}\begin{bmatrix} F_{n_1} \\ F_{n_2} \end{bmatrix} + \frac{1}{\beta}\begin{bmatrix} \beta_1 + 2r^2 & \beta_1 + 2r^2 \\ \beta_1 + 2r^2 & \beta_1 + 2r^2 \end{bmatrix}\begin{bmatrix} F_{\tau_1} \\ F_{\tau_2} \end{bmatrix} + \begin{bmatrix} -0.5l\dot{\theta}^2 \\ 0.5l\dot{\theta}^2 \end{bmatrix} \tag{43}$$

where $\beta = m_b l^2 + 4J_b + 2J_r$, $\beta_1 = \beta/(2m_b + m_r)$, $\beta_2 = \beta_1 + (4m_b + m_r)l^2/(4m_b + 2m_r)$, $\beta_3 = \beta_1 - 0.5l^2$.

Obviously, both matrices **C** and **D** in (43) are not full rank due to $\theta = 0$. If both the tips keep slipping, the friction forces F_{τ_1} and F_{τ_2} in Eq.42 can be represented by the the normal forces based on the Coulomb's friction law, so the singularity of the matrices **C** and **D** has no influence on the simulation. Then, Eq.42 can be expressed as Eq.31 with a positive definite matrix $\hat{\mathbf{A}}$, that can be solved by using the complementarity conditions in Eq.20. However, if both the tips keep sticking on the plate, i.e. $\dot{x}_{\tau_1} = 0$ and $\dot{x}_{\tau_2} = 0$, the superstatic problem of rigid body model will occur due to the singularity of the matrix **D** in (43). In this case, the tangential forces cannot be expressed as the form in (38) since the inverse matrix of **D** does not exist. Nevertheless, detailed observation for Eq.43 can provide a way of dealing with the singularity. The sum of the two equations in (43) gives:

$$\ddot{x}_{\tau_1} + \ddot{x}_{\tau_2} = \frac{2rl}{\beta}[F_{n_2} - F_{n_1}] + \frac{2(\beta_1 + 2r^2)}{\beta}[F_{\tau_1} + F_{\tau_2}] \tag{44}$$

and their substraction gives:

$$\ddot{x}_{\tau_1} - \ddot{x}_{\tau_2} = l\dot{\theta}^2 \tag{45}$$

By setting $\ddot{x}_{\tau_1} = \ddot{x}_{\tau_2} = 0$, we can immediately obtain $\dot{\theta} = 0$, and

$$F_{\tau_1} + F_{\tau_2} = \frac{rl}{\beta_1 + 2r^2}[F_{n_1} - F_{n_2}] \tag{46}$$

It is noteworthy that $\dot{\theta} = 0$ implies a solution in the stick mode. Moreover, we can write Eq.42 as:

$$\begin{bmatrix} \ddot{x}_{n_1} \\ \ddot{x}_{n_2} \end{bmatrix} = \frac{1}{\beta}\begin{bmatrix} \beta_2 & \beta_3 \\ \beta_3 & \beta_2 \end{bmatrix}\begin{bmatrix} F_{n_1} \\ F_{n_2} \end{bmatrix} + \frac{1}{\beta}\begin{bmatrix} -rl \\ rl \end{bmatrix}(F_{\tau_1} + F_{\tau_2}) + \begin{bmatrix} -g \\ -g \end{bmatrix} \tag{47}$$

Substitution of Eq.46 into (47) leads to

$$\begin{bmatrix} \ddot{x}_{n_1} \\ \ddot{x}_{n_2} \end{bmatrix} = \frac{1}{\beta}\begin{bmatrix} \beta_2 - \frac{(rl)^2}{\beta_1+2r^2} & \beta_3 + \frac{(rl)^2}{\beta_1+2r^2} \\ \beta_3 + \frac{(rl)^2}{\beta_1+2r^2} & \beta_2 - \frac{(rl)^2}{\beta_1+2r^2} \end{bmatrix}\begin{bmatrix} F_{n_1} \\ F_{n_2} \end{bmatrix} + \begin{bmatrix} -g \\ -g \end{bmatrix} \tag{48}$$

Using Eq.48 and the complementarity condition one can obtain the values of F_{n_1} and F_{n_2} as well as $F_{\tau_1} + F_{\tau_2}$ by Eq.46. As a result from the knowledge that the two contact points in one rigid body should slip or stick on the plate simultaneously, we can define the following *correlation coefficient of friction*,

$$\mu_{st} = \frac{|F_{\tau_1} + F_{\tau_2}|}{F_{n_1} + F_{n_2}} \tag{49}$$

Obviously, at the instant of $\dot{x}_{\tau_1} = 0$ and $\dot{x}_{\tau_2} = 0$, the transition from slip to stick can be identified by the following relationships. If

$$\mu_{st} < \min(\mu_{s_i}), \quad i = 1, 2 \tag{50}$$

a transition from slip to stick will occur, $\dot{\theta} = 0$, $\dot{x}_{\tau_1} = \dot{x}_{\tau_2} = 0$, and $\dot{x}_{n_1} = \dot{x}_{n_2} = 0$ can be considered as the solution of the dimer dynamics. If

$$\mu_{st} > \max(\mu_{s_i}), \quad i = 1, 2, \tag{51}$$

the tangential constraint for stick should be replaced by the one for slip, and the LCP's equations should be reformed to obtain the correct contact forces. If the dimer is previously located in a stick mode, the identification for a transition from stick to slip takes a similar process.

4 Impact dynamics with friction

4.1 Impulsive differential equations

When $\delta_1 = 0$ or $\delta_2 = 0$, or both, and when the relative normal velocity $\dot{\delta}_i < 0$, a collision between the ball and the plate occurs. Roughly speaking, there exist two different kinds of impact events: single impacts and double impacts. The single impact occurs when one tip is airborne while the other tip collides against the plate. The double impacts correspond to the situation when one tip of the dimer lies on the plate at the instant of the other tip colliding against the plate, or both collide at the same time.

According to the Darboux-Keller's method [3, 49, 16, 45, 47, 48], an impact process should experience a course at the impulse level even though it can be thought of an instantaneous event. Let $[t_0, t_f]$ denote the time interval of the impact, which can be further divided into much smaller intervals $[t_i, t_{i+1}]$. Assuming that positions $\mathbf{q}$ are constant on $[t_0, t_f]$ and that all forces are negligible w.r.t. the contact forces $\mathbf{F}_n$, $\mathbf{F}_\tau$, the integration for the dynamical equations of the dimer over $[t_i, t_{i+1}]$ results in a set of differential equations with respect to the normal impulses

$$\int_{t_i}^{t_{i+1}} [\mathbf{M}\ddot{\mathbf{q}} - \mathbf{h} - \mathbf{K^T F} - \mathbf{Q_g}]dt \quad = \mathbf{M} \cdot d\dot{\mathbf{q}} - \mathbf{K^T} \cdot d\mathbf{P} = 0 \tag{52}$$

where the vectors $\mathbf{h}$ and $\mathbf{Q_g}$ are non-impulsive terms and therefore vanish by the integration. The quantities $d\dot{\mathbf{q}} = \dot{\mathbf{q}}(t_{i+1}) - \dot{\mathbf{q}}(t_i)$ and

$$d\mathbf{P} = \int_{t_i}^{t_{i+1}} \mathbf{F}dt = \int_0^{t_{i+1}} \mathbf{F}dt - \int_0^{t_i} \mathbf{F}dt = \mathbf{P}(t_{i+1}) - \mathbf{P}(t_i), \tag{53}$$

are the changes of generalized velocities and normal impulses on $[t_i, t_{i+1}]$, respectively. From (13), the local impact dynamics at the impulse level can be expressed as:

$$\begin{bmatrix} d\dot{\mathbf{x}}_n \\ d\dot{\mathbf{x}}_\tau \end{bmatrix} = \mathbf{KM^{-1}K^T} \cdot \begin{bmatrix} d\mathbf{P}_n \\ d\mathbf{P}_\tau \end{bmatrix} \tag{54}$$

and can be further separated as

$$d\dot{\mathbf{x}}_n = \mathbf{A} \cdot d\mathbf{P}_n + \mathbf{B} \cdot d\mathbf{P}_\tau \tag{55}$$

and

$$d\dot{\mathbf{x}}_\tau = \mathbf{C} \cdot d\mathbf{P}_n + \mathbf{D} \cdot d\mathbf{P}_\tau \tag{56}$$

where $d\dot{\mathbf{x}}_n = [d\dot{x}_{n_1}, d\dot{x}_{n_2}]^T$, $d\dot{\mathbf{x}}_\tau = [d\dot{x}_{\tau_1}, d\dot{x}_{\tau_2}]^T$, $d\mathbf{P}_n = [dP_{n_1}, dP_{n_2}]^T$, $d\mathbf{P}_\tau = [dP_{\tau_1}, dP_{\tau_2}]^T$, and $\mathbf{KM^{-1}K^T} = \begin{pmatrix} A & B \\ C & D \end{pmatrix}$.

4.2 The normal and tangential constraints for impacts

Contacting bodies during impacts will experience a complex process with energy dissipation and dispersion [30]. Basically speaking, the dissipation of energy can be defined by using Stronge's coefficient of restitution [15], and the dispersion of energy appearing in a multi-impact process can be described by using a distributing law, which will be illustrated in the next subsection. According to Stronge's definition, the dissipated energy at the contact point i experiencing an impact with a single compression/expansion cycle can be defined by

$$e_{s,i}^2 = -\frac{W_{r,i}}{W_{c,j}} = -\frac{\int_{P_{n_i}(t_c)}^{P_{n_i}(t_f)} \dot{\delta}_i dP_{n_i}}{\int_0^{P_{n_i}(t_c)} \dot{\delta}_i dP_{n_i}} \tag{57}$$

where $W_{c,i} \leq 0$ and $W_{r,i} \geq 0$ are the works done by the normal contact force at point j during the compression phase $[0, t_c]$ and the expansion phase $[t_c, t_f]$, respectively. $\dot{\delta}_i$ is the relative normal velocity at the contact point i. One has

$$\dot{\delta}_i = \dot{x}_{n_i} - \dot{y}_p(t), \quad i = 1, 2. \tag{58}$$

Obviously $W_{c,i}$ also corresponds to the potential energy accumulated during the compression phase, and can be obtained by summing the scalar product of dP_i and $\dot{\delta}_i$ from the beginning of the impact to the instant of $P_i(t_c)$ that corresponds to $\dot{\delta}_i(t_c) = 0$. Thus

$$P_{n_i}(t_c) = \int_0^{t_c} dP_{n_i}, \qquad \dot{\delta}_i(P_{n_i}(t_c)) = 0 \tag{59}$$

and

$$W_{c,i} = \int_0^{P_{n_i}(t_c)} dP_{n_i} \dot{\delta}_i, \qquad \dot{\delta}_i(P_{n_i}(t_c)) = 0 \tag{60}$$

After that, the potential energy will be transferred into kinetic energy through the expansion phase. Since $e_{s,i}$ can always be identified off-line (as a function of $W_{c,i}$), the total recovered energy $W_{r,i}$ can be determined by $e_{s,i}$ and $W_{c,i}$. For instance, $W_{r,i}$ equals $W_{c,i}$ for a fully elastic impact, and $W_{r,i} = 0$ for a plastic impact.

The energetic coefficient of restitution can be extended to the situation where there exists some initial potential energy ($E_{0,i} < 0$) at the contact point i [47],

$$e_{s,i}^2 = -\frac{W_{r,i}}{E_{0,i} + W_{c,i}} \tag{61}$$

Eq.61 presents a normal constraint at the energy level to consider the transition of energy during an impact:

The dissipated energy during an impact process depends on the initial energy $E_{0,i}$ and the input energy $W_{c,i}$ at the contact point, as well as the coefficient of restitution $e_{s,i}$.

Let us denote $E_i(P_{n_i}(t))$ the residual potential energy at any instant t associated with a normal impulse $P_{n_i}(t)$ for the contact point i. According to [47], $E_i(P_i(t))$ can be expressed as

$$E_i(P_{n_i}(t)) = E_{0,i} + \frac{1}{Tra} \int_0^{P_{n_i}(t)} \dot{\delta}_i dP_{n_i} \tag{62}$$

where Tra is a parameter to transfer the work done by the normal impulse into the potential energy: $Tra = 1$ for a compressional phase ($\dot{\delta} < 0$), and $Tra = e_i^2$ for an expansion phase ($\dot{\delta} > 0$). Obviously, the impact finishes at the instant when no potential energy exists at the contact point i, i.e.

$$E_i(P_{n_i}(t)) = 0, \quad i = 1, 2. \tag{63}$$

Eq.63 can be thought of as a normal constraint for an impact event that is defined at the energy level. The constraint in the tangential direction during an impact event is still governed by the Coulomb's friction law, which can be equivalently rewritten at the impulsive level as:

$$dP_{\tau_i} = -\mu_i \, dP_{n_i} sign\left(\frac{\mathbf{v}_{\tau_i}}{\mid \mathbf{v}_{\tau_i} \mid}\right), \text{ , if } \mathbf{v}_{\tau_i} \neq 0, i = 1, 2 \tag{64}$$

$$dP_{\tau_i} = -\mu_i \, dP_{n_i} sign\left(\frac{\dot{\mathbf{v}}_{\tau_i}}{\mid \dot{\mathbf{v}}_{\tau_i} \mid}\right), \text{ if } \mathbf{v}_{\tau_i} = 0 \text{ and } \dot{\mathbf{v}}_{\tau_i} \neq 0, \tag{65}$$

$$\mid dP_{\tau_i} \mid \leq \mu_{s_i} dP_{n_i}, \text{ if } \mathbf{v}_{\tau_i} = 0 \text{ and } \dot{\mathbf{v}}_{\tau_i} = 0, \tag{66}$$

It is noteworthy that Coulomb's law in Eq.64-66 is written for the infinitesimal impulses, and thus does not suffer from the energetical problems of friction laws written at the impulse level [3, §4.2].

4.3 The distributing law for multiple impacts

In case of a single impact (only one contact point during the impact), the normal impulse at the contact point varies monotonically, and thus can be taken as a "time-like" independent variable [49, 16, 45, 12, 47] for the impulsive differential equations (54). Then the output of the system after an impact (the post-impact velocity of the system) can be obtained by integrating the differential equations (54) at the impulsive scale. However, when impacts involve multiple contacts, the energy will disperse and propagate in space through the network of contacts. In this case, the normal impulses at every contact point are tangled with each others and the process of multiple impacts is complex. In order to establish the relationship among the normal impulses at every contact point, a distributing law and the relevant numerical scheme are developed in [47, 48] for dealing with the event of multiple impacts without friction. The basic idea is the following:

The material properties of the contacting bodies can be represented by a compliance model composed of a compression (or loading) phase and an expansion (unloading) phase. Suppose that the contact point i takes the following force/indentation relationship for a compressional phase

$$F_{n_i} = K_i(\delta_i)^{\eta_i}, \quad i = 1, 2 \tag{67}$$

where $\eta_i = 3/2$ for Hertz's contact, K_i is the contact stiffness, and F_{n_i} is the contact force during the compression phase, δ_i is the relative displacement between the contacting bodies as expressed in Eq.16. The force/indentation relationship in the expansion phase is connected with (67) by using an energetic coefficient $e_{s,i}$ to take into account the dissipation of energy. After that, we can transfer the relationship of

force/displacement into the level of impulse-velocity to link the normal contact force F_{n_i} to the potential energy $E_i(P_{n_i}(t))$ stored at the contact point i

$$\frac{dP_{n_i}}{dt} = F_{n_i}(P_{n_i}(t)) = (1+\eta)^{\frac{\eta_i}{\eta_i+1}} K_i^{\frac{1}{\eta_i+1}} (E_i(P_{n_i}(t)))^{\frac{\eta_i}{\eta_i+1}} . \tag{68}$$

Since the contact forces can always be expressed as the differential of the normal impulse with respect to time, from (68) and assuming the exponent η_i in the force/indentation relationship takes equal values η at all contacts, the ratios between the increments of normal impulses among various contact points i can be expressed as

$$\frac{dP_{n_i}}{dP_{n_j}} = \gamma_{ij}^{\frac{1}{\eta+1}} (E_{ij}(P_{n_i}, P_{n_j}))^{\frac{\eta+1}{\eta}}, \quad i = 1, 2, i \neq j \tag{69}$$

where $\gamma_{ij} = K_i/K_j$ and $E_{ij} = E_i/E_j$ are the ratios of the contact stiffnesses and the potential energies between contact points i and j. Eq.69 represents the variation of normal impulse during the same time interval, and is termed as a *distributing law* related to the increments of the normal impulses dispersed in space [47].

It is obvious that (69) establishes a relationship between various normal impulses to make the impulsive differential equations (54) with a unique independent "time-like" variable. Combining this distributing law with the impulsive differential equation makes frictionless multiple impacts solvable. For the selection of the independent "time-like" variable, a guideline can be found in [47], in which the event of multiple impacts is dominated by a *primary contact point* that corresponds to the point taking the maximal potential energy among the various contacts.

4.4 The topology of impacts with friction

Usually, the friction at contact points has little influence on the normal compliance law. Therefore, the distributing law discovered for frictionless multiple impacts can be extended to the frictional case. Similarly to the case of contacts with friction, the structure of the impulsive differential equations (52) may be changed due to the participation of friction, depending on the tangential constraints defined by the Coulomb's law from (64) to (66). For instance, the relationship between the normal and tangential impulses at the same contact point will change when the contact status varies from slip to stick or *vice versa*. In this subsection, the possible structure of the impact dynamics for the dimer is discussed.

4.4.1 A single impact with friction

Let us assume the left steel ball ($i = 1$) collides against the oscillated plate, while the right ball is airborne. Thus $dP_{\tau_2} = 0$ and $dP_{n_2} = 0$. From the local impulsive differential equation (55) one obtains

$$\begin{bmatrix} d\dot{x}_{n_1} \\ d\dot{x}_{n_2} \end{bmatrix} = \mathbf{A} \cdot \begin{bmatrix} dP_{n_1} \\ 0 \end{bmatrix} + \mathbf{B} \cdot \begin{bmatrix} dP_{\tau_1} \\ 0 \end{bmatrix} \tag{70}$$

During an impact process, the matrices $\mathbf{A}$ and $\mathbf{B}$ are supposed to be constant due to the negligible variation of the configuration. Let us set the contact point ($i = 1$) with slip (i.e. the relative tangential velocity $\mathbf{v}_{\tau_1} = \dot{x}_{\tau_1} \neq 0$). The tangential impulse dP_{τ_1} satisfies the Coulomb's friction law:

$$dP_{\tau_1} = -\mu_1 dP_{n_1} sign(\dot{x}_{\tau_1}). \tag{71}$$

Thus, we have

$$d\dot{x}_{n_1} = \hat{A}_1 dP_{n_1} \tag{72}$$

where $\hat{\mathbf{A}}$ is in Eq.32. The impulsive differential equations can be advanced according to the "time-like" independent variable dP_{n_1}. The end of the impact will be monitored by using the residual potential energy at the contact point. If

$$E_1(P_{n_1}(t)) = \frac{1}{Tra}\int_0^{P_{n_1}(t)} \dot{\delta}_1 dP_{n_1} = 0, \quad \text{and} \quad \dot{\delta}_1 > 0, \tag{73}$$

is detected at the instant of P_{n_1}, the impact at the contact point 1 finishes and the generalized velocities can be obtained from Eq.52 that can be thought of as the output of the impact to reinitialize the system and advance the numerical scheme to the next step.

During the impact, the event of $\dot{x}_{\tau_1} = 0$ may be checked before $E_1(P_{n_1}) = 0$. This event may change the structure of the impulsive differential equations due to the variation of the property of the tangential constraint. Similarly to the case of the point in contact with the plate, we can set $d\dot{x}_{\tau_1} = 0$ for Eq.56,

$$\begin{bmatrix} 0 \\ d\dot{x}_{\tau_2} \end{bmatrix} = \mathbf{C} \cdot \begin{bmatrix} dP_{n_1} \\ 0 \end{bmatrix} + \mathbf{D} \cdot \begin{bmatrix} dP_{\tau_1} \\ 0 \end{bmatrix} \tag{74}$$

It is noteworthy that $\mathbf{C}$ and $\mathbf{D}$ are also constant, and a relationship between the tangential and normal impulses can be obtained:

$$dP_{\tau_1} = \widetilde{\mu}^1_{st} dP_{n_1}. \tag{75}$$

Let us denote a *correlation coefficient of friction*

$$\mu^1_{st} = |\widetilde{\mu}^1_{st}|. \tag{76}$$

If $\mu^1_{st} < \mu_{s_1}$, the friction at the instant of $\dot{x}_{\tau_1}(P_{n_1}(t_k)) = 0$ obeys Coulomb's law for stick. Then Eq.75 can be substituted into (70) to express the impulsive differential equation with respect to the normal impulse dP_{n_1}. However, if $\mu^1_{st} > \mu_{s_1}$, the contact point will keep slipping on the oscillated plate. In this case, the relationship between the tangential and normal impulses is

$$dP_{\tau_1} = -\mu_1 dP_{n_1} sgn(d\dot{x}_{\tau_1}), \tag{77}$$

then Eq.77 can be substituted into (70), and the the simulation can be advanced based on the tangential constraint expressed in (77).

Let us compare the correlative coefficients of friction in contact and impact phases at a single contact point with friction. From Eq.28, the relationship between the friction and normal forces is influenced by the terms from the external and initial forces, thus the value of μ^1_{st} will vary even though the contact point keeps sticking. However, the correlative coefficient of friction for impacts will be only influenced by the configuration that is constant due to the assumptions of impulsive dynamics. Therefore, for an impact in the dimer, the coefficient μ^1_{st} is a constant with respect to a certain configuration. This also implies that the stick mode will be preserved once it is triggered (detailed information related to a single impact with friction is given in [45, 12]).

4.4.2 Double impacts with friction

The double impacts in the dimer occur when one tip hits the oscillating plate, while the other contact is closed. In this case, two normal impulses will appear in Eq.52. During double impacts, the potential energies accumulated in the two contact points will vary and then make the *primary contact point* be altered. Let us set i as the primary contact point, in which

$$E_i \geq E_j, \quad i \neq j, \quad \text{and} \quad i, j = 1, 2. \tag{78}$$

Thus dP_{n_i} can be thought of as the primary normal impulse taken as an independent variable. The variation of the normal impulse at the contact point j, dP_{n_j}, can be connected with dP_{n_i} by the distributing law

$$dP_{n_j} = \gamma_{ji}^{\frac{1}{\eta+1}} (E_{ji}(P_{n_i}, P_{n_j}))^{\frac{\eta+1}{\eta}} dP_{n_i} \tag{79}$$

For the case of the two contact points with the same Hertz's contact ($\eta = 3/2$), Eq.79 can be written as

$$dP_{n_j} = (E_{ji}(P_{n_i}, P_{n_j}))^{\frac{5}{3}} dP_{n_i} \tag{80}$$

If both contact points are slipping ($\dot{x}_{\tau_i} \neq 0$, $\dot{x}_{\tau_j} \neq 0$), then

$$dP_{\tau_i} = -\mu_i \, dP_{n_i} sign(\dot{x}_{\tau_i}), \quad dP_{\tau_j} = -\mu_j \, dP_{n_j} sign(\dot{x}_{\tau_j}) \tag{81}$$

Substitution of (79) and (81) into Eq.55 leads to

$$\begin{bmatrix} d\dot{x}_{n_1} \\ d\dot{x}_{n_2} \end{bmatrix} = \hat{\mathbf{A}} dP_{n_i} \tag{82}$$

Thus, the impulsive differential equations can be solved before the tangential constraints at the contact points are changed. The end of the double impact is monitored by the potential energies accumulated in the two contact points. If the potential energies at the contact points satisfy

$$E_j(P_{n_j}(t)) = 0, \quad \text{and} \quad E_i(P_{n_i}(t)) \neq 0, \tag{83}$$

the impact at point j finishes. The double impact becomes a single impact at the contact point i. Only if both the potential energies at the two contact points satisfy $E_i = 0$ and $E_j = 0$, the double impact will be completed.

Let us investigate the possible variation of the tangential constraints during double impacts. We assume that the event $\dot{x}_{\tau_i} = 0$ is checked, but at the other contact point $\dot{x}_{\tau_j} \neq 0$, before the impacts at the two points finish ($E_i \neq 0$ and $E_j \neq 0$). Thus, the tangential constraint applied on the contact point i may be varied and should be identified correctly. From Eq.56 with the distributing law (79) and the tangential constraint for slip at point j, $dP_{\tau_j} = -\mu_j sgn(\dot{x}_{\tau_j}) dP_{n_j}$, we can obtain:

$$d\dot{x}_{\tau_i} = \hat{C}_i dP_{n_i} + \hat{D}_i dP_{\tau_i} \tag{84}$$

for some $\hat{C}_i$ and $\hat{D}_i$. Setting $d\dot{x}_{\tau_i} = 0$ leads to

$$dP_{\tau_i} = -\frac{\hat{C}_i}{\hat{D}_i} dP_{n_i} \tag{85}$$

Let us denote $\mu_{st}^i = |\hat{C}_i/\hat{D}_i|$ the correlative coefficient of friction in this situation. If $\mu_{st}^i < \mu_{s_i}$, Eq.85 can be substituted into (56) to make it solvable with respect to the independent normal impulse dP_{n_i}. If $\mu_{st}^i > \mu_{s_i}$, the tangential constraint at the contact point j should be replaced by the Coulomb's friction law for slip, $dP_{\tau_j} = -\mu_j \; sgn(d\dot{x}_{\tau_j}) dP_{n_j}$, and then it can be substituted into (56) to obtain the solution of the impulsive differential equations.

In the case of both contact points with zero tangential velocities ($\dot{x}_{\tau_i} = 0$, $i = 1, 2$) before impacts finish ($E_i \neq 0$ and $E_j \neq 0$), we can set $d\dot{\mathbf{x}}_\tau = 0$ in Eq.56 and use the distributing law (79) to obtain the following relationship,

$$d\mathbf{P}_\tau = -\mathbf{D}^{-1}\hat{\mathbf{C}} dP_{n_i} \tag{86}$$

From Eq.86, two correlative coefficients of friction related to the ratios between the corresponding normal and tangential impulses at the two contact points can be obtained.

$$\mu_{st}^i = \frac{|dP_{\tau_i}|}{dP_{n_i}}, \quad \text{and} \quad \mu_{st}^j = \frac{|dP_{\tau_j}|}{dP_{n_j}} \tag{87}$$

If

$$\mu_{st}^i < \mu_{s_i}, \quad \text{and} \quad \mu_{st}^j < \mu_{s_j}, \tag{88}$$

both contact points will satisfy the tangential constraints from the Coulomb's friction law for stick. Then we can substitute (86) into Eq.56 to obtain the impulsive differential equations with the same form as shown in Eq.82, but the elements of the matrix $\hat{\mathbf{A}}$ in this case will take different values in comparison with the ones in Eq.82.

If one of the conditions in (88) cannot be satisfied, the tangential constraint at the corresponding point should be replaced by the Coulomb's friction law for slip. Let us assume that

$$\mu_{st}^i > \mu_{s_i}, \quad \text{and} \quad \mu_{st}^j < \mu_{s_j}. \tag{89}$$

Then the tangential constraint at the contact point i should be

$$dP_{\tau_i} = -\mu_i \; dP_{n_i} sgn(d\dot{x}_{\tau_i}). \tag{90}$$

It is noteworthy that the value of μ_{st}^j will also be influenced by the property of the tangential constraint at the contact point i. Therefore, we should first substitute the tangential slip constraint at contact point i into Eq.56 to obtain a similar relationship as shown in Eq.84. By setting $d\dot{x}_{\tau_j} = 0$ we can obtain a correct relationship between the normal and tangential impulses (dP_{n_j} and dP_{τ_j}) for the contact point j with stick mode. After that, the correct tangential constraints at both contact points can be substituted into Eq.56 to obtain the impulsive differential equations with the similar form as shown in Eq.82, which can be solved by using the independent normal impulse dP_{n_i}.

If both the conditions in (88) are not satisfied, in which

$$\mu_{st}^i > \mu_{s_i} \quad \text{and} \quad \mu_{st}^j > \mu_{s_j}. \tag{91}$$

then the contact points should take the tangential constraints of the Coulomb's friction for slip.

$$dP_{\tau_i} = -\mu_i \, dP_{n_i} sgn(d\dot{x}_{\tau_i}), \quad dP_{\tau_j} = -\mu_j \, dP_{n_j} sgn(d\dot{x}_{\tau_j}) \tag{92}$$

A similar form as in Eq.82 for the impulsive differential equations with respect to the independent normal impulse dP_{n_i} can be obtained.

4.5 The singularity in double impacts and the inelastic collapse

As illustrated in section 3, a singularity will appear in the case of two contact points sticking on the plate. Basically speaking, the dynamics in contact and impact phases takes the same structure generated by the variation of the tangential constraints at contact points except for the nonimpulsive terms. Therefore, such a a singularity will also be induced by impacts, and requires a detailed analysis.

Due to the special configuration of the dimer, double impacts occur when $\theta = 0$, and the matrix $\mathbf{D}$ is singular. Therefore, when both contact points take zero tangential velocities ($\dot{x}_{\tau_i} = 0$, $i = 1, 2$) before double impacts finish ($E_i \neq 0$ and $E_j \neq 0$), we cannot obtain the relationship between the tangential impulses $d\mathbf{P}_\tau$ and the normal impulses $d\mathbf{P}_n$ according to Eq.86.

Following the reasoning in section 3 that deals with the singularity of the dimer contacting the plate with two stick contact points, we can obtain

$$dP_{\tau_1} + dP_{\tau_2} = \frac{rl}{\beta_1 + 2r^2}[dP_{n_1} - dP_{n_2}], \tag{93}$$

by setting $d\dot{x}_{\tau_1} = 0$ and $d\dot{x}_{\tau_2} = 0$. Let us assume that dP_{n_1} is the primary normal impulse, then dP_{n_2} can be connected with dP_{n_1} by the distributing law in Eq.69. Thus, we can use the fact that the two contact points have to slip or stick on the plate simultaneously to define a correlation coefficient of friction for the singularity in double impacts:

$$\mu_{st} = \frac{|dP_{\tau_1} + dP_{\tau_2}|}{dP_{n_1} + dP_{n_2}}, \tag{94}$$

which can be further expressed as

$$\mu_{st} = \frac{rl}{\beta_1 + 2r^2} \cdot \frac{|1 - \gamma_{21}^{1/(\eta+1)} E_{21}^{(\eta+1)/\eta}|}{1 + \gamma_{21}^{1/(\eta+1)} E_{21}^{(\eta+1)/\eta}}. \tag{95}$$

At the instant of $\dot{x}_{\tau_1} = 0$ and $\dot{x}_{\tau_2} = 0$, if

$$\mu_{st} < \min(\mu_{s_i}), \quad i = 1, 2 \tag{96}$$

the tangential constraint in the two contact points should satisfy the relationship expressed in Eq.93. Then we can substitute it into the following impulsive equations obtained from Eq.55 for $\theta = 0$

$$\begin{bmatrix} d\dot{x}_{n_1} \\ d\dot{x}_{n_2} \end{bmatrix} = \frac{1}{\beta} \begin{bmatrix} \beta_2 & \beta_3 \\ \beta_3 & \beta_2 \end{bmatrix} \begin{bmatrix} dP_{n_1} \\ dP_{n_2} \end{bmatrix} + \frac{1}{\beta} \begin{bmatrix} -rl \\ rl \end{bmatrix} (dP_{\tau_1} + dP_{\tau_2}), \tag{97}$$

and obtain the following impulsive differential equations with respect to the independent normal impulse dP_{n_1},

$$\begin{bmatrix} d\dot{x}_{n_1} \\ d\dot{x}_{n_2} \end{bmatrix} = \frac{1}{\beta} \begin{bmatrix} \beta_2 - \frac{(rl)^2}{\beta_1+2r^2} & \beta_3 + \frac{(rl)^2}{\beta_1+2r^2} \\ \beta_3 + \frac{(rl)^2}{\beta_1+2r^2} & \beta_2 - \frac{(rl)^2}{\beta_1+2r^2} \end{bmatrix} \begin{bmatrix} 1 \\ \gamma_{21}^{\frac{1}{\eta+1}} E_{21}^{\frac{\eta+1}{\eta}} \end{bmatrix} \cdot dP_{n_1} \tag{98}$$

If

$$\mu_{st} > \max(\mu_{s_i}), \quad i = 1, 2, \tag{99}$$

the tangential constraint at the two contact points is:

$$dP_{\tau_i} = -\mu_i \, dP_{n_i} sgn(d\dot{x}_{\tau_i}), \quad i = 1, 2, \tag{100}$$

Substituting Eq.100 into (97) can also lead to the impulsive differential equations with respect to the normal impulse dP_{n_1}. It is obvious that the impulsive differential equations in both cases can be solved by taking dP_{n_1} as a "time-like" independent variable. The end of the impact at each contact point will be controlled by the normal constraint defined at the energy level.

A sequence of impacts can be transferred into a contact phase, which is related to the problem of *inelastic collapse* studied by many authors [59, 57, 58]. For instance, an inelastic ball will physically come to rest in a finite time. However, if the collision for each bounce is assumed instantaneous and inelastic with constant Newton's restitution coefficient, the theoretical results will show that an infinite number of bounces occurs. Obviously this phenomenon cannot be expected experimentally, and is named *collisional singularity*.

The misconstruction for the problem of the inelastic collapse is due to the Newton's restitution coefficient used for describing an impact process. Let us recall the schemes in dealing with a system with or without a shock action. The main difference between them is whether the nonimpulsive forces are ignored or not. The usual method for an impact is that the effects from the nonimpulsive forces is omitted like the way of using the Newton's restitution coefficient to obtain the post-impact velocity after each bounce. When the intensity of an impact is very small, it is obvious that the nonimpulsive forces will significantly influence or dominate the behavior of the system. Thus their effects cannot be ignored. For the typical example of the inelastic ball bouncing on the ground, the reason for its rest is due to the gravity applied on it, but not the complete dissipation of energy. In other words, when the contact between the ball and the ground is established, a part of the energy will be resided in the ball to generate a vibration. This has been verified by the experiments in [57]. Therefore, a transition from a sequence of impacts to a contact will be significantly influenced by the relative effects between the contact and nonimpulsive forces. A simple way of identifying the transition from a sequence of impacts to a contact can be defined by the following condition,

$$\delta_i = 0, \ \dot{\delta}_i < 0, \ \text{ and } \ |\dot{\delta}_i| < \epsilon, \tag{101}$$

where ϵ is a small quantity. We assume that the contact is closed if the output of impacts for the relative velocity between the plate and the tip is $|\dot{\delta}_i| < A\omega/100$.

5 Qualitative analysis for the drift motion in the bouncing dimer

According to the precise experiments presented in [38], the dimer bouncing on an oscillated plate can exhibit a horizonal drift motion in certain initial and driving conditions. Obviously the formation of the ordered behavior significantly depends on the impact and contact dynamics of the dimer. Based on the qualitative analysis for the experimental findings, in this section we will investigate the driving mechanism of the drift motion, and then estimate the stick coefficient of friction between the dimer and the plate.

5.1 Experimental phenomenon in the dimer

Two experimental results are presented in [38] for the dimers with respective aspect ratios $A_r = 3.9$ and $A_r = 5.7$. In both cases the dimer will exhibit different drift motions: for small A_r, a positive drift motion is generated, in which the direction of the drift will be towards the bouncing end; for large A_r, however, the dimer is directed towards its staying end, and a so-called negative drift motion is generated.

Detailed observation of the experimental curves in Fig.3(b) [38], clearly shows that the dimer in both cases will experience the following different modes in every cycle of the drift motion: *double impacts* in which the bouncing sphere collides against the oscillated plate while the other ball stays on the plate; *a short-term free motion* of the dimer after the double impacts; *a sequence of single impacts* between the staying ball and the plate; *a contact phase* in which the staying ball lies on the oscillated plate. These different modes make a cycle for the drift motion that is repeated to drive the dimer moving horizontally.

Nevertheless, the different aspect ratios of A_r will make the drift motion with different horizonal directions (see Fig.3(a) in [38]), and the tangential velocities at the staying ball will take different characteristics (see Fig.3(b) in [38]). In the case of small A_r, the horizonal velocity can suddenly vary from a negative value to a positive one at the event of double impacts, while for large A_r, the value of the horizontal velocity seems to be always null after the event of the double impacts. During the phase of the sequence of single impacts, the horizonal velocity in the case of small A_r decreases gradually, while the horizonal velocity in the case of large A_r seems to be null for a relatively long time. Detailed examination in [38] shows that contact between the staying ball and the oscillated plate can also be established in both cases, in which a transition from stick to slip appears in the case of large A_r, while a reverse slip appears in the case of small A_r.

From the observation for the experimental finding, it is clear that the difference of the drift motions between the small and large A_r is due to the frictional behavior at the contact point, which strictly depends on the relationship between the *correlation coefficient of friction* and the stick coefficient of friction.

5.2 The correlative coefficient of friction

When a tip has a zero tangential velocity in both the contact and impact phases, the tangential constraint depends on the property of the friction cone at the contact point, that can be identified by using a correlation coefficient of friction. This coefficient represents a relationship between the tangential and normal contact forces, which can

be satisfied for the contact point in a stick mode. For the contact point with a slip mode, however, the relationship between the normal and tangential forces should be redefined by using a constant slip coefficient of friction. Let us first consider the correlative coefficient of friction in the case of the dimer with one contact point at i.

From Eq.25, the tangential acceleration at the contact point i can be explicitly expressed as

$$\ddot{x}_{\tau_i} = \frac{\beta_1 + \beta_4 + \beta_5}{\beta} F_{\tau_i} - \frac{\beta_6}{\beta} F_{n_i} + H_{\tau_i} \tag{102}$$

where

$$\beta_4 = \frac{(m_b + 0.5m_r)l^2 \sin^2\theta}{2m_b + m_r}, \quad \beta_5 = 2rl\sin\theta + 2r^2, \quad \beta_6 = (0.5l^2\sin\theta + rl)\cos\theta. \tag{103}$$

and β_1 is in Eq.43. By setting $\ddot{x}_{\tau_i} = 0$, we have

$$F_{\tau_i} = \frac{\beta_6}{\beta_1 + \beta_4 + \beta_5} F_{n_i} - \frac{\beta}{\beta_1 + \beta_4 + \beta_5} H_{\tau_i} \tag{104}$$

The correlative coefficient of friction is $\mu_{st}^{i,C}$ and can be expressed as

$$\mu_{st}^{i,C} = \frac{1}{\beta_1 + \beta_4 + \beta_5} |\beta_6 - \beta H_{\tau_i}/F_{n_i}| \tag{105}$$

Then, we can compare the values of $\mu_{st}^{i,C}$ and of the static coefficient of friction μ_{s_i} to identify the tangential status at the contact point i. Obviously, the value of $\mu_{st}^{i,C}$ is influenced not only by the configuration, but also by H_{τ_i} coming from non-contact forces.

Similarly, from Eq.75 and (76), we can denote the correlative coefficient of friction in the case of contact point i with a single impact as $\mu_{st}^{i,I}$, that can be explicitly expressed as

$$\mu_{st}^{i,I} = \frac{\beta_6}{\beta_1 + \beta_4 + \beta_5}, \tag{106}$$

which is only associated with the configuration of the dimer at the instant of $\dot{x}_{\tau_i} = 0$. When more contacts are closed, the calculation for μ_{st}^{i} depends on the tangential contact status at other points, which has been discussed in sections 3 and 4 for the contact and impact phases, respectively.

The event of double impacts seems to play a significant role for the formation of the drift motion in the dimer. Let us denote the correlative coefficient of friction in this case as μ_{st}^{DI}. From Eq.95 and setting the tips in the left and right balls with the same Hertz' contact ($\gamma_{21} = 1$ and $\eta = 3/2$), we have

$$\mu_{st}^{DI} = \frac{rl}{\beta_1 + 2r^2} \frac{|1 - (E_{12})^{\frac{5}{3}}|}{(E_{12})^{\frac{5}{3}} + 1} \tag{107}$$

It is noteworthy that the value of μ_{st}^{DI} will be influenced by the ratio of the potential energy E_{12} at the instant when $\dot{x}_{\tau_1} = \dot{x}_{\tau_2} = 0$. Moreover, since $E_{12} \leq 1$, one has

$$\mu_{st}^{DI} < \frac{rl}{\beta_1 + 2r^2} = \mu_{st}^{i,I}(\theta = 0), \tag{108}$$

which implies that at the same configuration the value of μ_{st}^{DI} must be less than the one of $\mu_{st}^{i,I}$.

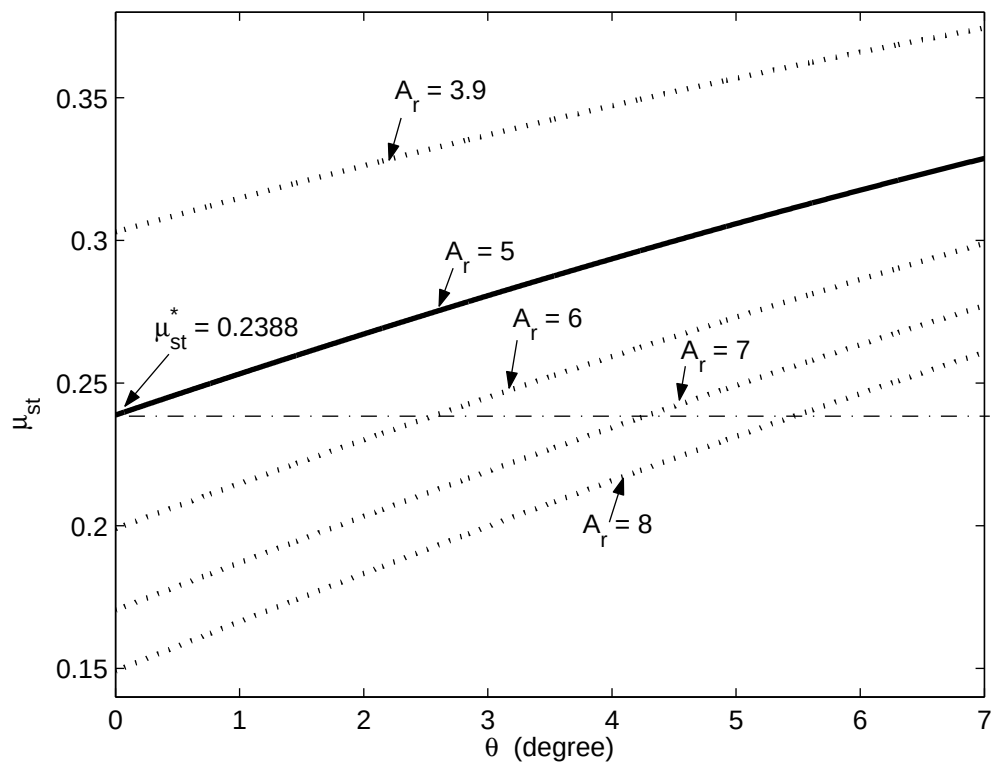

Figure 2: the value of μ_{st} with the variation of A_r and the angle θ.

5.3 Estimation of the coefficient of friction

Let us number 1 and 2 the respective quantities in the left and right balls. When the dimer moves with a drift mode, the term H_{τ_1} is related to $\dot{\theta}^2$ that is very small, and thus has little effects on the value of $\mu_{st}^{1,C}$. During the double impacts, the value of E_{12} is also very small since the left ball lies on the oscillated plate when double impacts occur. So we can approximately adopt a unified value of $\mu_{st} = \mu_{st}^{1,I}$ to identify the property of the tangential constraint, which is only associated with the configuration of the dimer (the tilt angle θ) and the geometrical parameter A_r. By setting the steel density $\rho_{steel} = 7.8 \times 10^3 kg/m^3$ and the glass density $\rho_{glass} = 1.0 \times 10^3 kg/m^3$, Figure 2 shows the evolution of μ_{st} with A_r and the angle θ.

Now, let us estimate the stick coefficient of friction according to the experimental findings in [38] and the unified correlative coefficient of friction μ_{st}. The experiments have shown that the dimer is directed towards the bouncing end if $A_r < 5$, otherwise, the dimer moves in the backward direction. As shown in the experimental curves (Fig.3(b) in [38]), the reason for this is due to the different behavior of the double impacts for small and large A_r. In the case $A_r = 3.9$, the horizonal velocity at the tip in the left ball can change with a positive value, while for the case $A_r = 5.7$ it is null.

If $A_r = 5$ is set as the critical value for the occurrence of the stick mode, it is obvious that the drift behavior of the dimer should also be changed before and after this value. Therefore, it seems reasonable that the value of μ_{st} at $A_r = 5$ and $\theta = 0$ should be assigned on the stick coefficient of friction μ_s since the drift direction is changed after

$A_r > 5$. From Eq.106 and the knowledge that the slip coefficient of friction is near to the half value of μ_s, we estimate that the coefficients of friction approximately take the following values

$$\mu_s \approx \mu_{st}(A_r = 5, \theta = 0) \approx 0.24, \quad \mu = \mu_{st}/2 = 0.12. \tag{109}$$

5.4 Qualitative analysis of the drift mode

Based on the estimation of the coefficient of friction and the theory developed in this paper, we can present a qualitative analysis for the experimental phenomena exhibited in the dimer. After double impacts, a sequence of small jumps will be excited due to the single impacts at the tip in the left ball, and then a contact phase between the left ball and the plate can be established. Obviously, these single impacts and the contact phase occur in the presence of friction, that may complicate the tangential constraint at the contact point.

From Fig.2, it is clear that the correlative coefficient of friction will vary not only with different A_r, but also will change with the tilt angle θ. Especially, for a fixed A_r its value will increase with the angle θ. Therefore, for a small aspect ratio $A_r < 5$, the dimer should keep the slip constraint of Coulomb's friction even though there exists an event of $\dot{x}_{\tau_1} = 0$ during the processes of a single impact or a contact phase. For the dimer with a large A_r, however, the correlative coefficient may be greater than the stick coefficient of friction when the dimer with a large tilt angle. Thus, the property of the tangential constraint at the tip of the dimer can be changed.

Since friction forces are linked to the direction of the slip velocity, the impulsive differential equations or the contact dynamical equations will be changed due to the different directions of the initial tangential velocity. So two cases associated with the initial tangential velocity of $\dot{x}^-_{\tau_1} > 0$ and $\dot{x}^-_{\tau_1} < 0$ should be separately investigated.

The impact initiated from $\dot{x}^-_{\tau_1} > 0$:

In the case $\dot{x}^-_{\tau_1} > 0$, the tangential constraint in a single impact at the tip of the left ball becomes $dP_{\tau_1} = -\mu dP_{n_1}$, and thus the tangential impulsive equations can be explicitly written as

$$d\dot{x}_{\tau_1} = -\frac{1}{\beta} \left[(\beta_1 + \beta_4 + \beta_5)\mu + \beta_6\right] dP_{n_1}. \tag{110}$$

Since the coefficient before dP_{n_1} is always negative, the tangential velocity $\dot{x}_{\tau_1}$ decreases during the impact initiated from $\dot{x}^-_{\tau_1} > 0$ and may reach zero. When the event $\dot{x}_{\tau_1} = 0$ is checked during the process of the impact, the tangential constraint at the tip will be changed depending on the value of A_r. For the dimer with an aspect ratio $A_r < 5$, the slip constraint of Coulomb's friction will be kept, but the slip direction may be changed. For the dimer with $A_r > 5$, if the event $\dot{x}_{\tau_1} = 0$ occurs when the tilt angle θ is small, the correlative coefficient will be smaller than the stick coefficient of friction, and thus the tangential constraint will be transferred into a stick mode that will make the tangential velocity at the contact point vanish when the impact finishes. If the event $\dot{x}_{\tau_1} = 0$ appears in the dimer with a large tilt angle, the correlative coefficient may be greater than the stick coefficient, thus a slip mode will appear in the dimer with $A_r > 5$.

The impact initiated from $\dot{x}^-_{\tau_1} < 0$:

If the single impact occurs when $\dot{x}_{\tau_1}^- < 0$, the tangential constraint at the contact point becomes $dP_{\tau_1} = \mu dP_{n_1}$, that will lead to the following tangential impulsive differential equation

$$d\dot{x}_{\tau_1} = -\frac{1}{\beta} \left[(\beta_1 + \beta_4 + \beta_5)\mu - \beta_6\right] dP_{n_1} \tag{111}$$

Obviously, the sign of the coefficient before dP_{n_1} will be influenced by the configuration of the dimer and the slip coefficient of friction. If

$$(\beta_1 + \beta_4 + \beta_5)\mu < \beta_6, \tag{112}$$

the tangential acceleration of $d\dot{x}_{\tau_1}$ is guaranteed to be greater than zero, thus may produce a discrete event $\dot{x}_{\tau_1} = 0$ for the impact initiated from $\dot{x}_{\tau_1}^- < 0$ and the tangential constraint will be changed during impacts. However, if

$$(\beta_1 + \beta_4 + \beta_5)\mu > \beta_6 \tag{113}$$

the tangential acceleration of $\dot{x}_{\tau_1}$ will be always less than zero during the process of the impact, thus no variation of the tangential constraint occurs for the impact initiated from $\dot{x}_{\tau_1}^- < 0$.

In order to qualitatively analyze the property of the tangential motion in the impact initiated from $\dot{x}_{\tau_1}^- < 0$, we can simplify the coefficient before dP_{n_1} by considering the dimer with a small tilt angle during the drift motion and ignoring the effects of the glass rod. Thus, we can set

$$\sin\theta \approx 0, \quad \cos\theta \approx 1, \quad m_r = 0, \quad J_r = 0, \tag{114}$$

and Eq.111 becomes

$$d\dot{x}_{\tau_1} = \frac{f(B_r)}{2(B_r^2 + 1.6)} dP_{n_1} \tag{115}$$

where $B_r = l/r$, and the function $f(B_r)$,

$$f(B_r) = \mu B_r^2 - 2B_r + 5.6\mu \tag{116}$$

The sign of the function $f(\cdot)$ depends on the roots of the equation $f(B_r) = 0$. Obviously, if $\mu > 1/\sqrt{5.6}$, no real root exists, so $d\dot{x}_{\tau_1} > 0$ is guaranteed that will make $\dot{x}_{\tau_1} \to 0$ during the single impact initiated from $\dot{x}_{\tau_1}^- < 0$.

If $0 < \mu < 1/\sqrt{5.6}$, there are two real roots:

$$B_{r_1} = \frac{2 - \sqrt{1 - 5.6\mu^2}}{2\mu}, \quad B_{r_2} = \frac{2 + \sqrt{1 - 5.6\mu^2}}{2\mu} \tag{117}$$

When $B_r \in [B_{r_1}, B_{r_2}]$, $d\dot{x}_{\tau_1} < 0$ and thus the amplitude of $\dot{x}_{\tau_1}$ will increase during the impact with an initial condition of $\dot{x}_{\tau_1}^- < 0$. So the discrete event of $\dot{x}_{\tau_1} = 0$ can not appear in the process of the single impact. If $B_r < B_{r_1}$ or $B_r > B_{r_2}$, the tangential velocity $\dot{x}_{\tau_1}$ will approach zero and a transition of the tangential constraint during the single impact is possible.

From the estimation of the slip coefficient of friction, $\mu = 0.12 < 1/\sqrt{5.6}$, and $B_r \in [B_{r_1}, B_{r_2}]$, this illustrates that the single impact initiated from $\dot{x}_{\tau_1}^- < 0$ cannot allow an event of $\dot{x}_{\tau_1}^- = 0$, and the tangential constraint is not changed.

Summary of the impact behavior at the left ball

If a single impact is initiated from $\dot{x}_{\tau_1}^- > 0$, the amplitude of the tangential velocity $\dot{x}_{\tau_1} > 0$ will decrease during impact and may trigger an event of $\dot{x}_{\tau_1} = 0$ before the impact finishes. For small A_r, the event of horizonal velocity vanishing will result in a reverse slip. For large A_r, this event will generate a stick mode when the tilt angle is small, and a reverse slip if the tilt angle is large enough. For the single impact initiated from $\dot{x}_{\tau_1}^- < 0$, the amplitude of the tangential velocity will increase until the impact finishes since the event of $\dot{x}_{\tau_1} = 0$ cannot occur.

The contact behavior at the left ball

A contact phase is confirmed by the detailed examination in [38] by measuring the electric resistance between the spheres and the plate, which is established by a sequence of single impacts. Obviously, the transition will occur if the intensity of the single impact is very small. During a (non impacting) contact phase, the tangential constraint at the contact point may also be changed due to the variation of the tangential velocity. Let us get back to the slip mode when the contact is closed, and assume $\dot{x}_{\tau_1} > 0$. Thus the tangential constraint is $F_{\tau_1} = -\mu F_{n_1}$. Similarly to the case of a single impact, the governing equation of the contact point in the tangential direction takes the following form,

$$\ddot{x}_{\tau_1} = -\frac{1}{\beta} \left[(\beta_1 + \beta_4 + \beta_5)\mu + \beta_6\right] F_{n_1} + H_{\tau_1} \tag{118}$$

The difference between (118) and (110) is that the tangential state in a contact phase will be influenced by H_{τ_1}. For the dimer with a drift motion, the value of H_{τ_1} is in general very small, such that the qualitative property of the tangential constraint in contact phases is similar to the case of the dimer experiencing a single impact. Therefore, for a dimer with a small A_r, the tangential velocity at the contact point will always decrease and can pass through zero to generate a reverse slip. However, for a dimer with a large A_r, when the tilt angle is very small, the tangential velocity will be restricted to $\dot{x}_{\tau_1} \geq 0$. Only when the tilt angle is large enough, the lock at the contact point can be released to permit a reverse slip.

For the case of the contact with the condition $\dot{x}_{\tau_1} < 0$, the governing equation in the tangential direction becomes

$$\ddot{x}_{\tau_1} = -\frac{1}{\beta} \left[(\beta_1 + \beta_4 + \beta_5)\mu - \beta_6\right] F_{n_1} + H_{\tau_1} \tag{119}$$

Clearly, the tangential state in this case is also influenced by the term H_{τ_1}. However, for the experimental parameters used in [38], it seems that the influences from H_{τ_1} is tiny and the property of the tangential constrained is kept the same as in the case of a single impact with an initial condition $\dot{x}_{\tau_1}^- < 0$.

Based on the above analysis, the behavior of the tangential velocities shown in Fig.3(b) [38], can be better understood. In the case $A_r = 3.9$, no stick mode can appear in the double impacts or the sequential single impacts and the contact phases.

So the tangential velocity can freely change without any restriction on its slip direction. Therefore, a positive tangential velocity can be obtained after double impacts, and will gradually decrease before its value equals zero, then increase its amplitude along a negative direction. Through a sequence of single impacts, a contact phase between the dimer and the plate can be established before or after the instant of $\dot{x}_{\tau_1} = 0$, and then a next cycle with a start of double impacts will begin: thus a positive drift motion is generated.

In the case $A_r = 5.7$, however, the double impacts will make the tangential post-impact velocity vanish due to the occurrence of the stick mode. After that a sequence of single impacts occurs and then a contact phase can be established when the intensity of impacts become much puny. In the situation of the dimer with a small tilt angle, the friction cone at the contact point only permits positive horizonal velocity, thus its value seems to be small or null for a relatively long time. Once the tilt angle is large enough, the restriction from the friction cone will be shaken off to admit a reverse slip. Then a negative slip can appear in the dimer.

6 comparison between numerical and experimental results

According to [38], the oscillated plate has a harmonic vibration with frequency f and amplitude A that is defined by a parameter Γ,

$$\Gamma = 4\pi^2 A f^2 / g \tag{120}$$

where g is the gravitational acceleration. Numerical simulation is also carried out in [38] based on an event-driven scheme with the following parameters: the Newton's coefficient of restitution $\epsilon = 0.65$; the stick and slip coefficients of friction for the contact phases $\mu_s = 0.4$ and $\mu = 0.2$; and the friction coefficients in impact phase $\hat{\mu}_s = 0.2$ and $\hat{\mu} = 0.1$. Although qualitative agreements between the numerical results and the experimental findings are achieved, there still exists a significant discrepancy at the quantitative level between the numerical results (see Fig.5 in [38]) with the experimental findings (Fig.3(b) in [38]). In this section, numerical simulations for the dimer under different initial and driving conditions are carried out by using the method proposed in this paper. The numerical results will be carefully compared with the experimental data provided in [38]. The influence of the parameters μ_s, μ and e_s on the numerical results will be discussed.

6.1 The preliminary numerical results

According to the estimation of the coefficient of friction presented in section 5.C, and the restitution coefficient used in [38], we adopt the following parameters to carry out the numerical simulations: $\mu_s = 0.24$, $\mu = 0.12$, $e_s = \epsilon = 0.65$. Let us first investigate the two cases exhibited in [38] for the dimer with $A_r = 3.9$ and $A_r = 5.7$. In both cases, the dimer is driven by the oscillated plate with the same parameters: $f = 25$Hz and $\Gamma = 0.9$. The initial configuration of the dimer is denoted by a tilt angle θ_0 and an initial height h_0, the distance between the tip (the potential contact point) in the lower end of the dimer and the equilibrium position of the oscillated plate. The simulation starts at the instant when the waveform of the plate oscillation is expressed as:

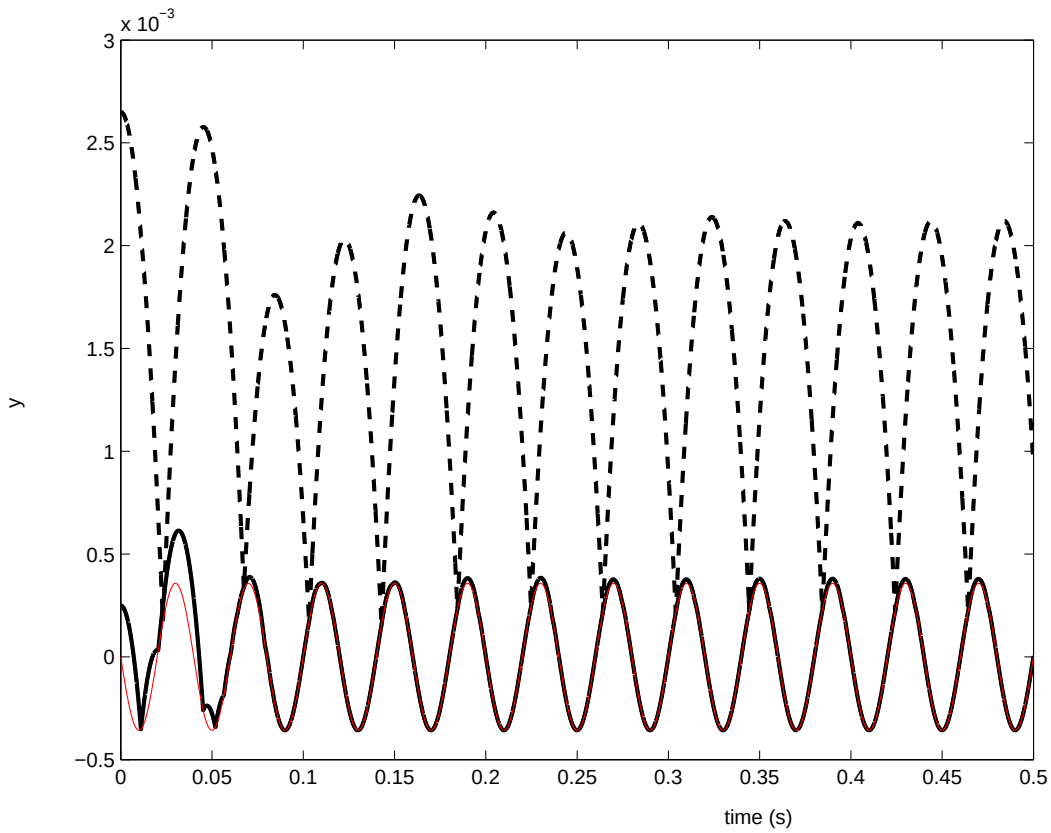

Figure 3: The vertical positions of the left (black solid line) and right (black dashed line) contact points of the dimer with $A_r = 3.9$ as a function of time obtained from numerical simulation, in which $f = 25$ Hz, and $\Gamma = 0.9$, $e_s = 0.65$, $\mu_s = 0.24$, $\mu = 0.12$. The red thin line is the vertical position of the plate.

$$y_p(t) = -A \sin \omega t \tag{121}$$

where $\omega = 1/f$ and A can be calculated according to the parameter Γ according to Eq.120.

For the dimer with $A_r = 3.9$, we compute $l = 2(A_r - 1)r = 27.55$mm. The initial conditions of the dimer are set as $\theta_0 = 5°$ and $h_0 = 0.25mm$. Fig.3 shows the numerical results for the vertical positions of the tips in the left (black solid line) and right (black dashed line) balls of the dimer. After several bounces to adjust the configuration of the dimer for participating impacts, a periodical vertical motion can be formed, in which the tip in the left ball of the dimer will stay on the plate, while the tip in the right ball will bounce off the plate periodically. The variation of the tilt angle is shown in Fig.4: it has approximately a constant amplitude.

Except for the normal periodic motion, a novel horizontal drift can be observed in Fig.5 for the tangential velocities at the left and right tips. From this figure we can clearly observe the scenario for the complex motion of the dimer experiencing the drift mode: after the initial free motion of the dimer, the left sphere will collide repeatedly

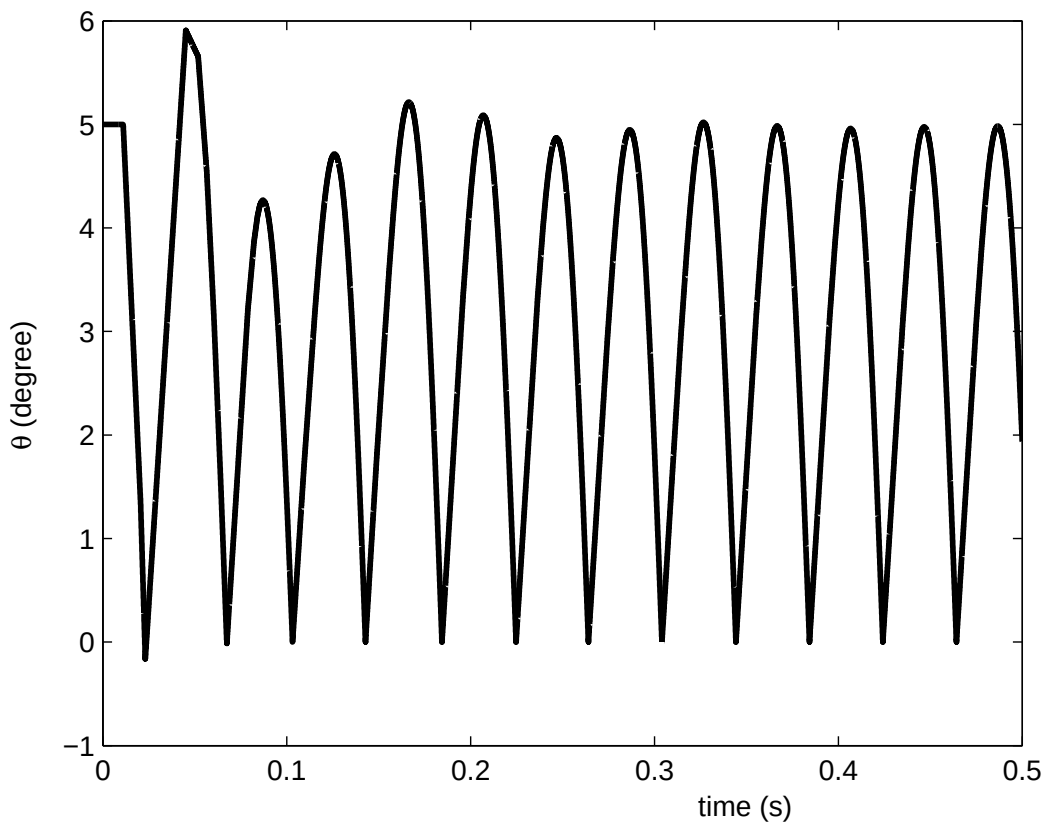

Figure 4: The numerical result of the swing angle θ obtained from the simulation parameters $e_s = 0.65$, $\mu_s = 0.24$, $\mu = 0.12$, for the dimer with $A_r = 3.9$, driving in $f = 25$ Hz, and $\Gamma = 0.9$.

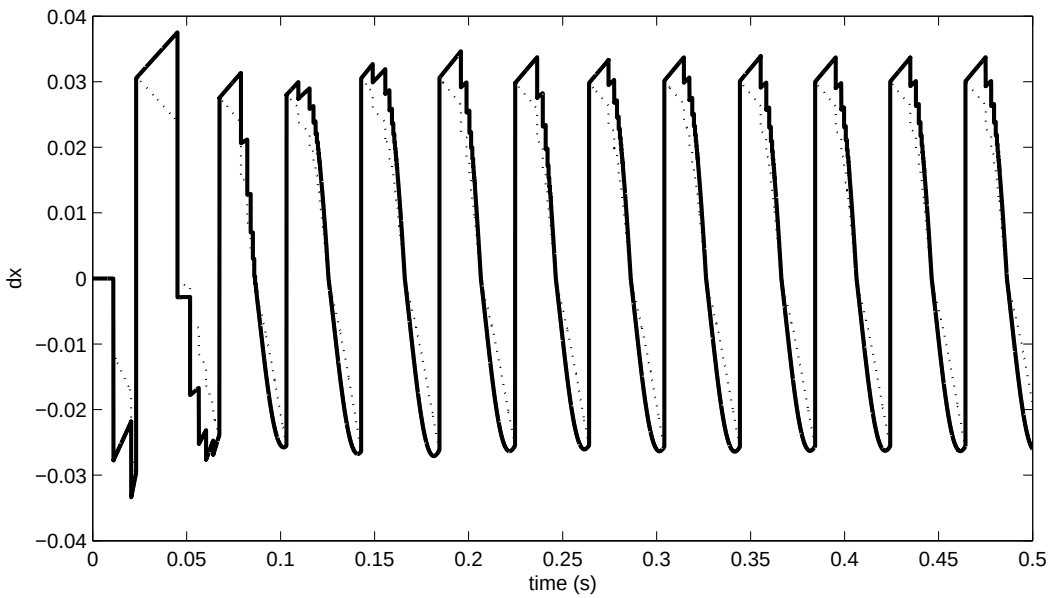

Figure 5: The tangential velocities of the left (solid line) and right (dashed line) tips for the dimer with $A_r = 3.9$ obtained from numerical simulation. The parameters for simulation are: $e_s = 0.65$, $\mu_s = 0.24$, $\mu = 0.12$, $f = 25$ Hz, and $\Gamma = 0.9$.

against the oscillated plate before the right ball reaches the plate. These single impacts will make the tangential velocities of both tips quickly decrease, while the tilt angle θ approaches zero (see Fig.4). After that, a strong collision between the right sphere and the plate occurs that makes the tangential velocities in both tips immediately change with a new positive direction. Then the right end of the dimer bounces far away from the plate, while the left end of the dimer experiences a sequence of single impacts. A next cycle for the right end of the dimer experiencing one collision *per* period of the plate oscillation begins.

Through the self-organization of the dimer motion experiencing a few cycles of the plate oscillation, the left ball will stay on the oscillated plate before the right ball collides against the plate. Then the single impact between the right ball and the plate will be transferred into double impacts. After that, a periodically complex motion will be formed that consists of double impacts, a sequence of single impacts at the left ball, and a contact phase between the left ball and the plate.

The evolution of the tangential velocities at the tips in the left and right balls shown in Fig.5 can also be better understood according to the qualitative analysis of the dimer dynamics. Since all the correlative coefficients in the dimer with $A_r = 3.9$ are smaller than the stick coefficient of friction μ_s, the tangential velocities at the tips can freely pass through zero when the contact between the dimer and the plate is closed. So no stick mode appears in the tangential constraints of the contact points, such that the double impacts can make the tangential velocities of both tips positive, and a single impact at the left ball can make its horizonal velocity decrease rapidly, while the contact between the left sphere and the plate can slip reversely.

It is obvious that the stable persistent drift motion is generated by the repeated complex motion that is periodic but rather subtle and much sophisticated in each cycle.

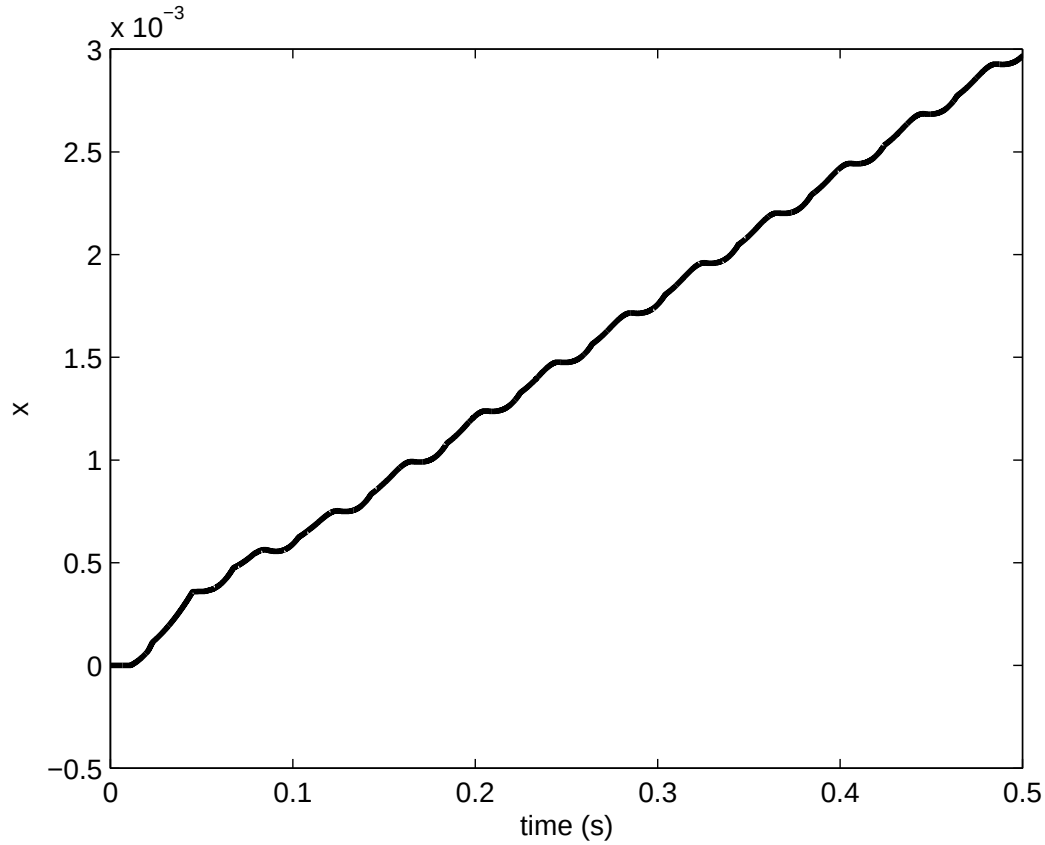

Figure 6: The horizontal position of the left tip of the dimer as a function of time in the drift mode for $A_r = 3.9$ obtained from the simulation parameters: $e_s = 0.65$, $\mu_s = 0.24$, $\mu = 0.12$, $f = 25$ Hz, and $\Gamma = 0.9$.

Fig.6 shows the horizontal position of the left tip of the dimer in the case $A_r = 3.9$. It is clear that the horizontal drift motion can be approximated as a uniform rectilinear motion with an approximately constant mean speed, $\langle u \rangle \approx 3.3$mm/s, obtained by dividing the distance x over ten cycles by the corresponding time.

In comparison with the experimental results for the dimer with $A_r = 3.9$ (see Fig.3 in [38]), a deviation at the quantitative level can be observed in the numerical results: the value of the mean drift speed obtained from simulation is lower than the one in experiments. From Fig.5, one finds that the horizonal displacement is synthesized by the positive and negative slip of the left tip in each cycle of the complicated periodic motion. Therefore, the difference between them will determine the magnitude of the mean drift speed, that will be influenced by the amplitudes of the positive and the negative horizonal speed, and the durations for each part. Since no stick mode appears in the tangential constraints for the dimer with $A_r = 3.9$, and these quantities will be affected by the slip coefficient of friction only. This illustrates that the estimated value $\mu = 0.12$ used in the simulation is not appropriate, and a modification for that will be discussed later.

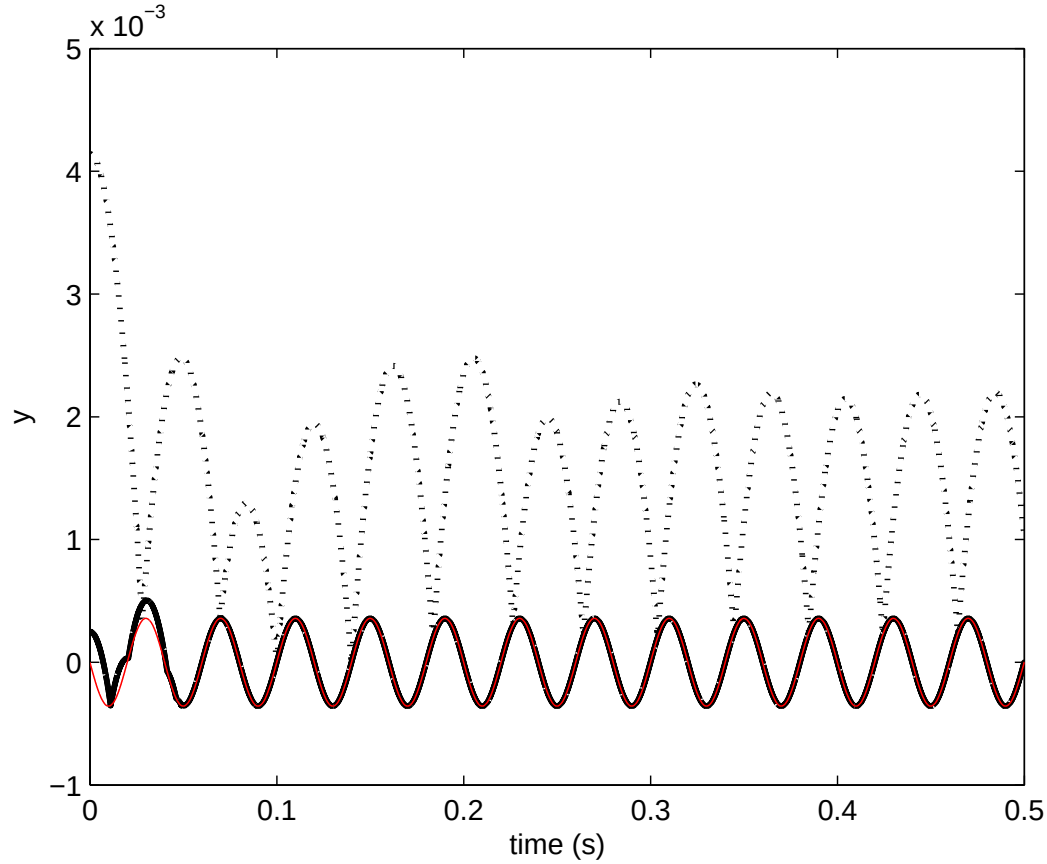

Figure 7: The vertical positions of the left (black solid line) and right (black dashed line) contact points of the dimer with $A_r = 5.7$ as a function of time obtained from numerical simulation, in which $f = 25$ Hz, and $\Gamma = 0.9$, $e_s = 0.65$, $\mu_s = 0.24$, $\mu = 0.12$. The red thin line is the vertical position of the plate.

Let us now investigate the case of the dimer with $A_r = 5.7$, in which it will be directed to drift backwards from the bouncing end (a negative direction). The initial conditions and the parameters used in simulation are the same as for the case $A_r = 3.9$: $h_0 = 0.25$mm, $\theta_0 = 5°$, $l = l = 2(A_r - 1)r = 44.65$mm, $\mu_s = 0.24$, $\mu = 0.12$, $e_s = 0.65$.

Similarly to the case $A_r = 3.9$, a periodic bouncing motion in the normal direction is observed in Fig.7, in which the bouncing end of the dimer will repeatedly collide against the oscillated plate, while the left sphere seems to stay on the plate. Fig.8 shows the variation of the swing angle θ that is also periodic with an approximately constant maximal swing angle.

However, the tangential motion of the dimer with $A_r = 5.7$ will significantly differ from the one with $A_r = 3.9$. Fig.9 depicts the evolution of the tangential velocities of the tips in the left and right balls for $A_r = 5.7$. Let us check the complex motion of the dimer in this case.

The correlative coefficient μ_{st} with a configuration $\theta = 5°$ is larger than the stick coefficient of friction. The initial single impact in the left sphere, after a free motion

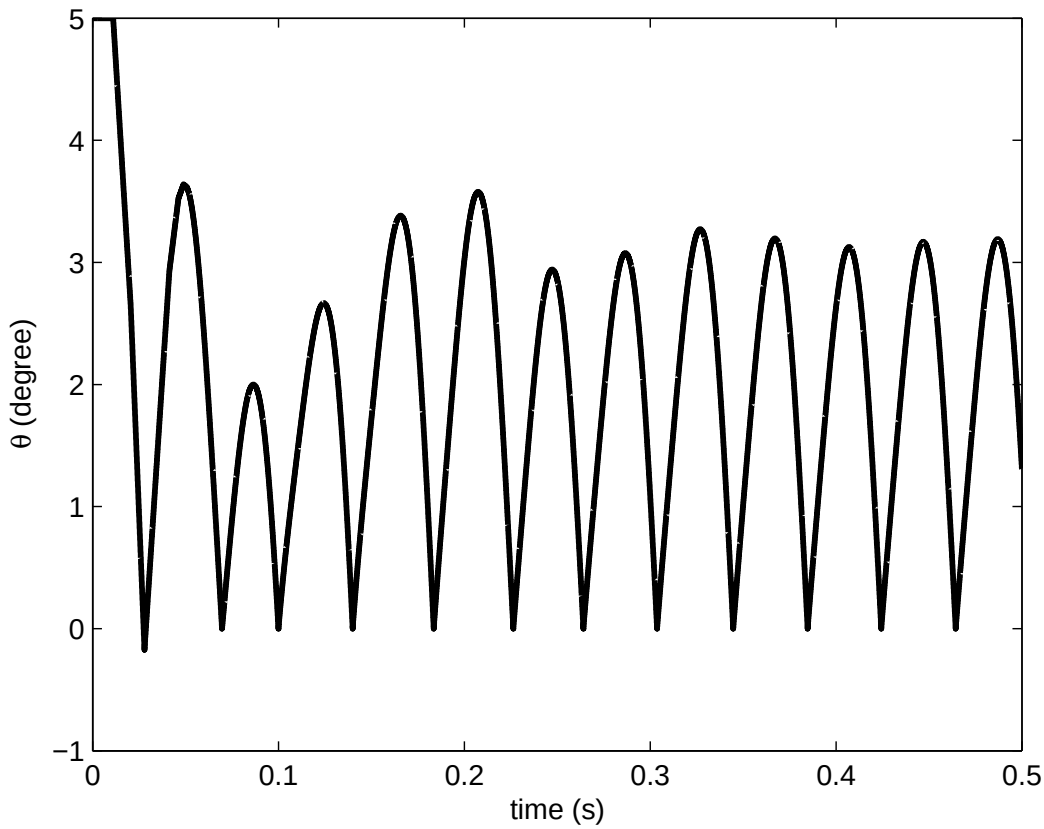

Figure 8: The numerical result of the swing angle θ obtained from the simulation parameters $e_s = 0.65$, $\mu_s = 0.24$, $\mu = 0.12$, for the dimer with $A_r = 5.7$, driving in $f = 25$ Hz, and $\Gamma = 0.9$.

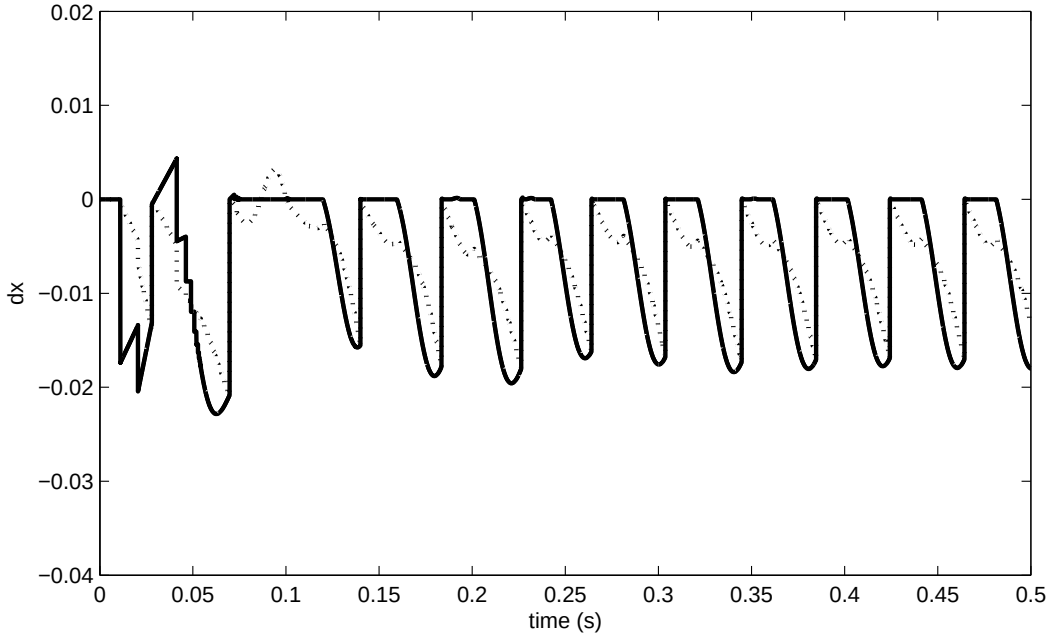

Figure 9: The tangential velocities of the left (solid line) and right (dashed line) tips for the dimer with $A_r = 5.7$ obtained from numerical simulation. The parameters for simulation are: $e_s = 0.65$, $\mu_s = 0.24$, $\mu = 0.12$, $f = 25$ Hz, and $\Gamma = 0.9$.

of the dimer, will therefore not take a stick mode in its tangential constraint. Consequently, the tangential velocity in the tip can change from zero to a negative value, and then the sequential detachment at the left ball will generate a sequence of single impacts that also makes the right ball approach the plate quickly. When the tilt angle θ is so small to make the correlative coefficient μ_{st} be less than the stick coefficient of friction μ_s, a stick mode will appear in the single impacts at the tips of the left and right balls. Thus the tangential post-impact velocities of the tips will vanish after the single impacts. Together with the decrease of the intensity in these single impacts, a contact between the left ball and the plate can be established. Then double impacts will appear in the dimer when the right ball reaches the plate again. Due to the stick mode in the tangential constraint, the tangential velocities at both tips of the left and right balls will be equal to zero after the double impacts. The sequential single impacts at the left ball will make its tangential velocity approximately null due to the stick mode of the tangential constraint. Once the tilt angle θ is large enough to make $\mu_{st} > \mu_s$, the stick mode at the tip of the left sphere will be shaken off, and the left ball can slip reversely. The repeated process will make the dimer drift backwards since the positive tangential velocity is absent in this case , see Fig.10.

It is obvious that the complex periodic motions in the dimer with respective $A_r = 3.9$ and $A_r = 5.7$ take a similar structure except for the variation of the tangential constraint during impacts and contact phases. Moreover, in comparison with the case $A_r = 3.9$, the numerical simulations shown in Fig.9 are close to the experimental results (see Fig.3 in [38]).

Let us present an explanation for the deviation between the numerical simulations and the experimental findings for the dimer with the two different aspect ratios. For the

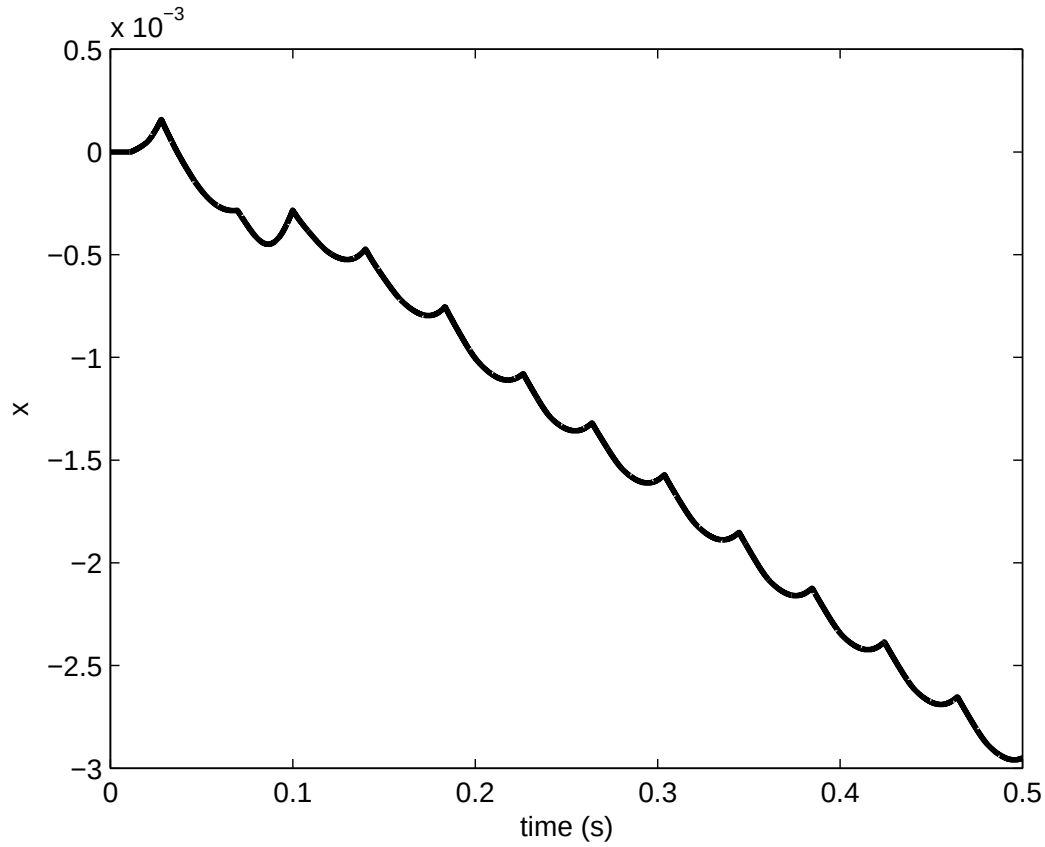

Figure 10: The horizontal position of the left tip of the dimer as a function of time in the drift mode for $A_r = 5.7$ obtained from the simulation parameters: $e_s = 0.65$, $\mu_s = 0.24$, $\mu = 0.12$, $f = 25$ Hz, and $\Gamma = 0.9$.

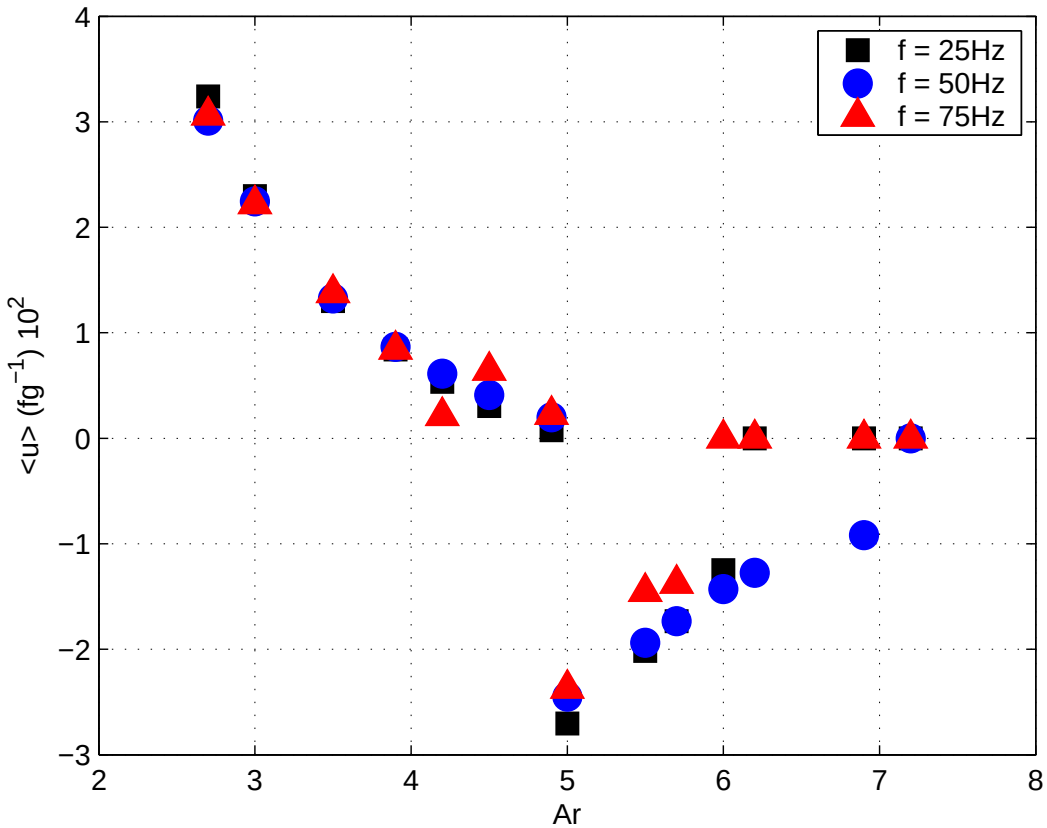

Figure 11: The mean horizontal speed of the dimer scaled by gravity and frequency versus A_r for three values of driving frequency. obtained from the simulation parameters: $e_s = 0.65$, $\mu_s = 0.24$, $\mu = 0.12$, $f = 25, 50, 75$ Hz, and $\Gamma = 0.9$.

dimer with $A_r = 5.7$, the mean drift motion mainly depends on the negative amplitude of the tangential velocity at the tip of the left sphere before the double impacts occur. The negative tangential velocity is generated by the slip rolling motion that starts from a stick mode in the left sphere. The small error between the numerical and experimental results illustrates that the slip coefficient of friction for a contact phase used in simulation is approximately correct. However, for the dimer with $A_r = 3.9$, the positive drift motion is synthesized by a positive and negative slip motions that depend on the property of the slip friction in double impacts. Therefore, we may postulate the following for the frictional behavior between bodies.

Claim: *Even though the stick coefficient of friction between bodies in impact and contact phases may take the same value, the slip coefficient of friction in impact phases should be less than the one in contact phases.*

It is not easy to give a rigorous support for this statement unless a lot of experiments are carried out. Intuitively, the strong interaction during impacts will weaken the tangential resistance due to the local plastic deformation, such that the slip coefficient of friction during impacts will be lessened. The numerical results obtained from a modification for the slip coefficient of friction will be presented in the next subsection.

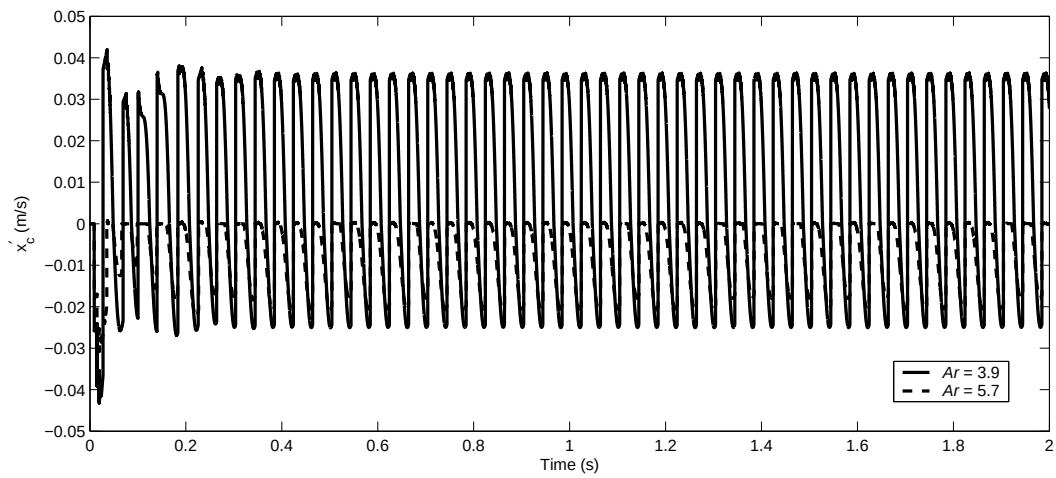

Figure 12: The horizonal velocities at the tip of the left ball in the dimer with $A_r = 3.9$ (solid line) and 5.7 (dashed line). The simulation parameters are: $f = 25$Hz, $\Gamma = 0.9$, $e_s = 0.65, \mu_s = 0.24, \mu^c = 0.12, \mu^i = 0.08$

Fig.11 shows the curves of the scaled mean horizontal speed versus A_r for the dimers driven by three different values of the frequency, $f = 25, 50, 75$Hz. The plate oscillation at each frequency shares the same parameter, $\Gamma = 0.9$. The scaled mean horizontal speed is denoted as $\langle u \rangle (fg^{-1})10^2$, where $\langle u \rangle$ is the mean horizonal speed obtained by dividing the drift distance over ten cycles with the corresponding time. It is noteworthy that the calculation of the mean drift speed is carried out only when a persistent motion of the dimer in drift mode is excited.

The scaled mean horizonal speed obtained from numerical results seems to well agree with the experimental results for the dimer with a negative drift motion (Fig.4(a) in [38]). However, quantitative errors between the numerical and experimental results exist in the cases of the dimer with a forward drift motion. For instance, the numerical simulation in Fig.11 shows that the mean drift speed monotonically varies with A_r, but the experimental findings indicate that the drift speed will take maximal at the neighborhood of $A_r = 3.5$. The discrepancy further illustrates that the modification for the value of μ during impacts is necessary.

Dorbolo et. al emphasized that their experiments do not show a discontinuous transition from forward to reverse drift at a certain A_r. Our numerical results clearly indicate that the forward drift will be transferred into the reverse one at $A_r = 5$ because the stick coefficient of friction μ_s takes the value of μ_{st} in the dimer with $A_r = 5$. They explained the discrepancy by the sensitivity of the double collision to small variations in frictional properties of the plate at large A_r. We believe the reason for that comes from the small variation of the stick coefficient of friction μ_s because of the age of contact when plenty of experiments are carried out.

6.2 Numerical results obtained by modifying the slip coefficient of friction

In order to reflect the difference of the frictional behaviors in contact and impact phases, let us denote as μ^i the slip coefficient of friction during impacts, and μ^c the one in

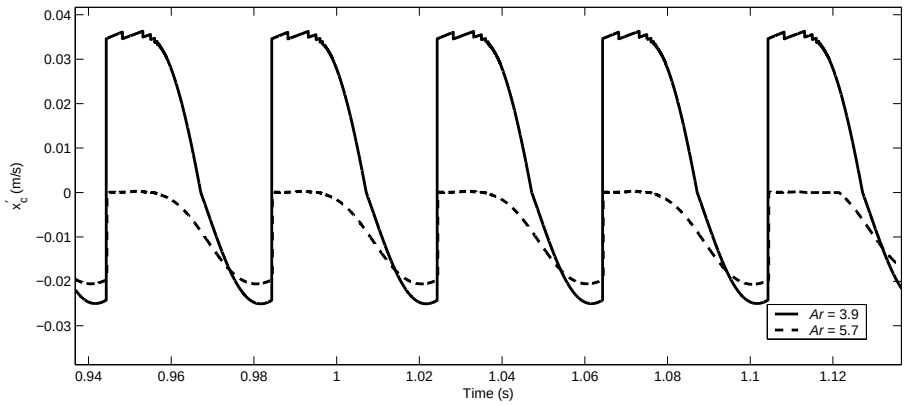

Figure 13: A local figure zoomed from Figure (12) for the horizonal velocity at the tip of the left ball in the dimer with $A_r = 3.9$ (solid line) and 5.7 (dashed line), respectively.

contacts. The slip coefficient of friction for contacts is kept as the value of $\mu^c = 0.12$, and the one in impacts is estimated from a fitting method with a value of $\mu^i = 0.08$ that can make the corresponding numerical simulation better coincide with the experimental results.

Under the same parameters as used in the above simulations except for the slip coefficient of friction during the impacts, Fig.12 shows the horizonal velocities at the tips of the left ball for the dimers with the aspect ratios of $A_r = 3.9$ and $A_r = 5.7$, respectively. Detailed observation for the horizonal velocities is presented in Fig.13, zoomed from Fig.12. Clearly, the new numerical results precisely agree with the experimental results Fig.3(a) in [38].

In comparison with the numerical results shown in Fig.5 for $A_r = 3.9$ obtained by setting $\mu^i = \mu^c = \mu = 0.12$, the new numerical results are significantly improved after the modification for the slip coefficient of friction in impacts. For the case of $A_r = 5.7$, the difference between the numerical results before and after the modification of the slip coefficient of friction is very small (see Fig.9 and 13).

The mean horizonal speed for the dimer with $A_r = 3.9$ and $A_r = 5.7$ can be calculated by the horizonal displacements at the tip of the left ball shown in Fig.14. In the case $A_r = 3.9$, the mean horizonal speed is $\langle u \rangle = 8.7mm/s$ and the horizonal distance at the left tip over $120ms$ is about $x_{\tau_1} = 1.044mm$. For the case of $A_r = 3.9$, $\langle u \rangle = -6.7mm/s$ approximately, and $x_{\tau_1} = -0.804mm$ over a timer interval $120ms$. Both of them are very close to the values shown in Fig.3(a) [38].

Let us check the influence of the aspect ratio A_r and the frequency f on the dynamics of the dimer in drift mode after the modification of the slip coefficient of friction. The simulations are carried out for the dimers with various A_r between 2.1 and 8.5 at three different frequencies of the plate vibration under the same energy $\Gamma = 0.9$. For each point shown in Fig.15, the scaled mean drift speed $\langle u \rangle$ is obtained when the persistent drift mode is excited by adjusting the initial conditions for the dimer releasing. When the plate oscillates with a low frequency f and the dimer with a small aspect ratio A_r, the excitation of the drift mode is more sensitive to the initial conditions. In particular, the drift mode cannot be excited for the dimer with $A_r < 2.1$ bouncing on the plate with $f = 25Hz$.

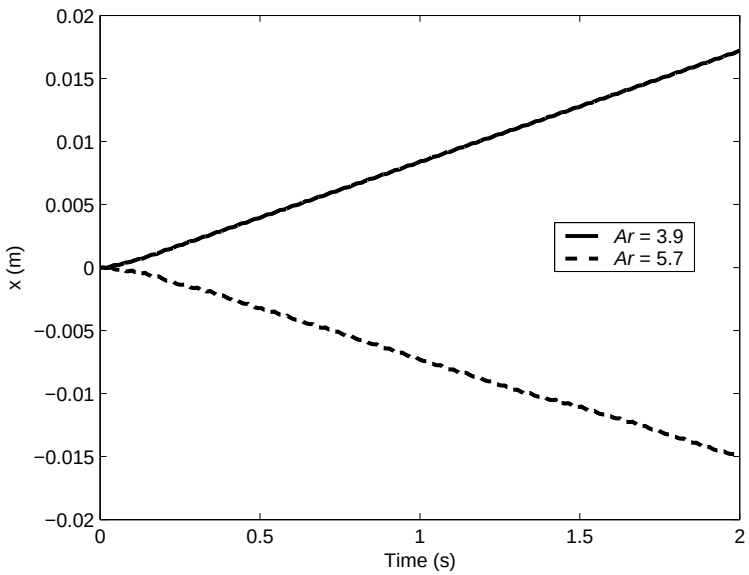

Figure 14: Horizonal displacements of the left tip of the dimer in the drift mode for $A_r = 3.9$ (solid line) and $A_r = 5.7$ (dashed line)

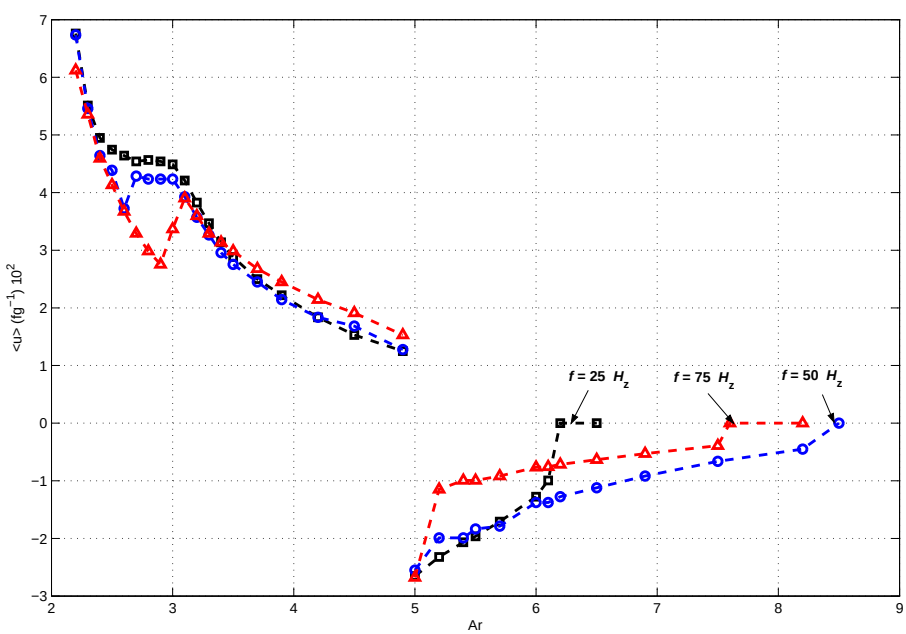

Figure 15: The scaled mean horizonal speed $\langle u \rangle (fg^{-1})10^2$ versus A_r for three values of driving frequency. Parameters used in simulations are: $\Gamma = 0.9$, $e_s = 0.65$, $\mu_s = 0.24$, $\mu^c = 0.12$, $\mu^i = 0.08$.

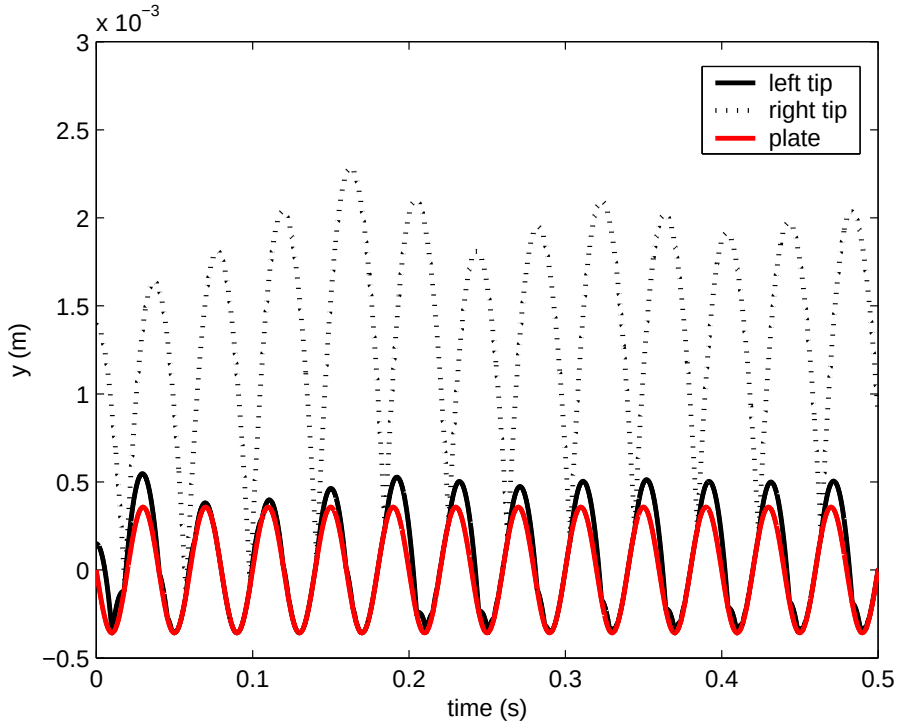

Figure 16: The vertical positions of the left (black solid line) and right (black dashed line) contact points of the dimer with $A_r = 2.5$ as a function of time obtained from numerical simulation, in which $f = 25$ Hz, and $\Gamma = 0.9$, $e_s = 0.65$, $\mu_s = 0.24$, $\mu^c = 0.12$, $\mu^i = 0.08$. The red thin line is the vertical position of the plate.

A persistent stable drift mode strictly depends on the periodic behaviors of the dimer bouncing on the plate, in which each cycle of the repeated bouncing motion consists of complex motions such as double impacts, a sequence of single impacts and the contacts with friction effects. In general, a stable repeated cycle can be formed only if the dimer is released with an initial condition defined in a special range. If the initial conditions are not appropriate, the drift mode cannot be generated. At this stage, it is still an open problem for finding the basin of attraction of stable periodic motions.

If $A_r < 2.5$, the drift mode becomes unstable according to the experimental observation in [38]. This can be explained by using the following numerical simulations for the dimer with $A_r = 2.5$ bouncing on the plate with $f = 25Hz$ and $\Gamma = 0.9$.

Figure 16 depicts the vertical positions at the tips of the left and right balls with $A_r = 2.5$. One sees that the left ball does not stay on the plate but leaves it with a small height. Fig.17 indicates that the contact phase between the left ball and the plate seems to be very short or absent during each cycle of the complicated periodic motion. Obviously, the absence of the contact phase in the left ball is the reason for the instability of the drift mode when $A_r < 2.5$. The unstable drift modes can also be found for the dimer with an aspect ratio near $A_r = 5$, in which there is a discontinuous transition from forward to backward drift motions. In these situations, the initial conditions for the release of the dimer should be carefully selected in order to form a stable drift mode.

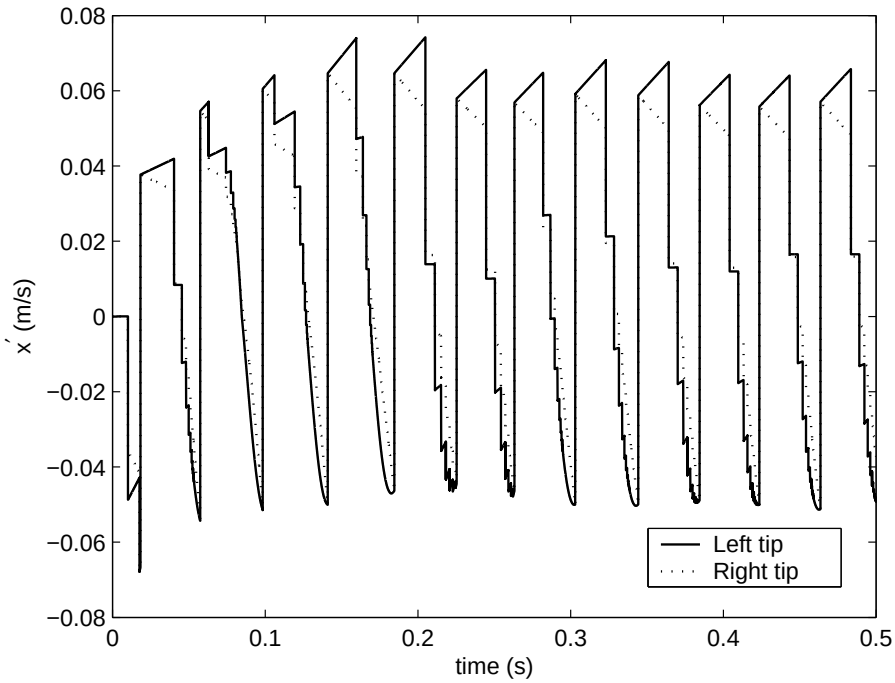

Figure 17: The tangential velocities of the left (solid line) and right (dashed line) tips for the dimer with $A_r = 2.5$ obtained from numerical simulation used in the following parameters: $f = 25$ Hz, and $\Gamma = 0.9$, $e_s = 0.65$, $\mu_s = 0.24$, $\mu^c = 0.12$, $\mu^i = 0.08$.

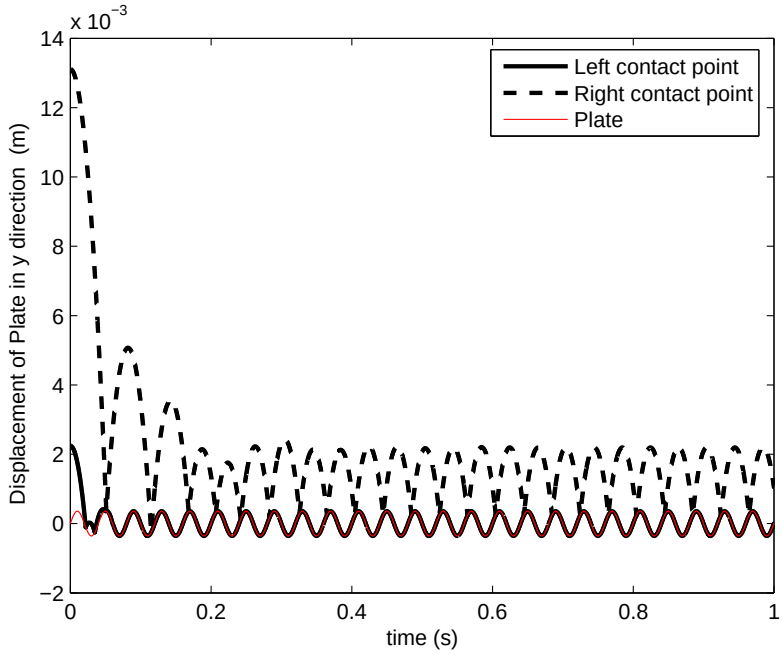

Figure 18: The vertical positions of the left (solid line) and right (dashed line) tips for the dimer with $A_r = 6.5$ obtained from numerical simulation used in the following parameters: $f = 25$ Hz, and $\Gamma = 0.9$, $e_s = 0.65$, $\mu_s = 0.24$, $\mu^c = 0.12$, $\mu^i = 0.08$.

From Fig.15, we can also find that the positive drift speed will decrease with the increase of the aspect ratio when $A_r \in (3.1, 5)$, and the value of the frequency has little influence on the scaled mean drift motion. Meanwhile, an inflexion exists at $A_r = 3.1$, in which the scaled mean drift speed in the case $f = 25Hz$ will rapidly decrease when A_r changes from 3.1 to 2.9, and then increases by further diminishing the value of A_r. In the cases of $f = 50$ and $75Hz$, the scaled mean drift speed seems to be a constant during the scope of $A_r \in (2.5, 3.1)$, and then rapidly increases when the value of A_r is further reduced.

In the case $A_r = 5$, a transition from forward to reversal drift motion will suddenly occur. Indeed the symmetric structure of the tangential velocity with small A_r (see the relevant figures for $A_r = 3.9$) collapses and is spontaneously transferred into the negative drift mode. Obviously, the symmetry breaking is due to the variation of the frictional behavior at the contact point. In the negative drift mode, the absolute value of the scaled mean drift speed will also decrease when A_r increases, and be significantly influenced by the value of the frequency of the plate. In the case $f = 25Hz$, the absolute value of the scaled mean drift speed will decrease rapidly, and vanish when $A_r > 6.2$. This situation is mostly like a single pendulum, in which one end of the dimer is fixed on the oscillated plate, and the other swings beyond the plate and collides against it once every cycle. Fig.18 shows the normal motion for the dimer with $A_r = 6.5$ released from an initial condition of $h_0 = 2.25mm$ and $\theta_0 = 12°$, in which a small swing appears in the right ball even though the mean drift speed equals zero.

In the cases of $f = 50$ and $75Hz$, the occurrence for the zero mean drift speed are $A_r = 8.2$ and 7.6, respectively. Under the same parameter Γ, the external and inertial forces applied in the dimer will vary with the frequency of the plate oscillation, thus the critical value for the occurrence of the single pendulum mode will be translated.

6.3 Other stable persistent motion shown in the dimer

For a fixed A_r, the mode of the persistent motion triggered in the dimer will be significantly influenced by the initial and driving conditions. For instance, the experiments in [38] clearly show that the dimer dynamics is sensitive to the initial conditions, and the transition from a drift mode to the higher energy jump and flutter modes could be observed when the parameter Γ related to the plate oscillation is varied. In the following, we carried out some numerical simulations and made an attempt to give an illustration for the transition between different modes.

Once a stable persistent motion is established, the total energy involved in the dimer should be approximately constant such that a quasi periodic motion holds. Let us analyze the energy involved in the drift, jump and flutter modes for the dimer.

In the case of the dimer with a stable drift mode, one ball stays on the plate, while the other ball swings beyond the plate and hits the plate once every cycle of the plate vibration. Most importantly, the swing motion of the dimer on the plate is much seemingly periodic and the maximal height of the hitting end at every cycle seems to be kept constant approximately. As a simple way for the estimation of the total mechanical energies involved in drift mode we simplify the dimer dynamics as a system of an elastic ball bouncing off a fixed ground, in which the time interval between two sequential bounces of the "elastic ball" is just equal to the period of the plate oscillation, T. The total mechanical energy in this simplified model is

$$E_d = mgh_{max} = mg \cdot \frac{1}{2}g(T/2)^2 = \frac{1}{8}mg^2T^2, \tag{122}$$

which can be thought of as the approximately constant energy involved in the dimer with a drift mode.

For the case of a jump mode, both the left and right balls will collide with the plate once every cycle of the plate oscillation. In this mode, the bouncing heights of the two balls are nearly the same. Since the glass rod is very light, the dimer resembles the situation of two separated particles bouncing on an oscillated plate with the same period that equals the period of the plate oscillation. From this simple model, the total mechanical energy of the dimer involved in the jump mode can be approximated as

$$E_j = 2mgh_{max} = 2mg \cdot \frac{1}{2}g(T/2)^2 = \frac{1}{4}mg^2T^2 \tag{123}$$

The scenario for the dimer with a flutter mode is that both the left and right balls hit the plate out of phase at every other period of oscillation. In this mode the time interval between two sequential bounces is approximately equal to twice the period of the plate oscillation. Therefore, when the mode is simplified as the situation of two separated particles bouncing on an oscillated plate with the same period, the total mechanical energy of the dimer involved in the flutter mode can be estimated by

$$E_f = 2mgh_{max} = 2mg \cdot \frac{1}{2}g(T)^2 = mg^2T^2 \tag{124}$$

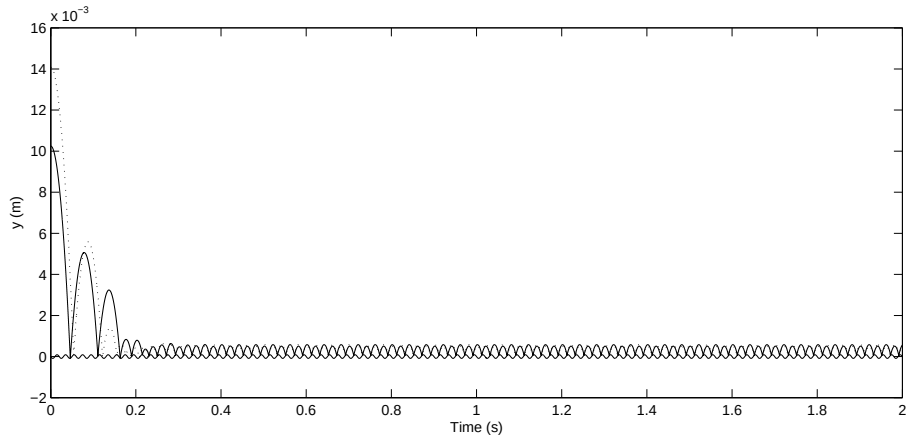

Figure 19: The vertical position of the tips in left (solid line) and right (dashed line) ball for the dimer ($A_r = 3.9$, $f = 50$Hz, $\Gamma = 0.9$) in a jump mode generated by an initial condition of $h_0 = 10.25mm$ and $\theta_0 = 8°$. Parameters of simulations are $e_s = 0.65$, $\mu_s = 0.24$, $\mu^c = 0.12$, $\mu^i = 0.08$.

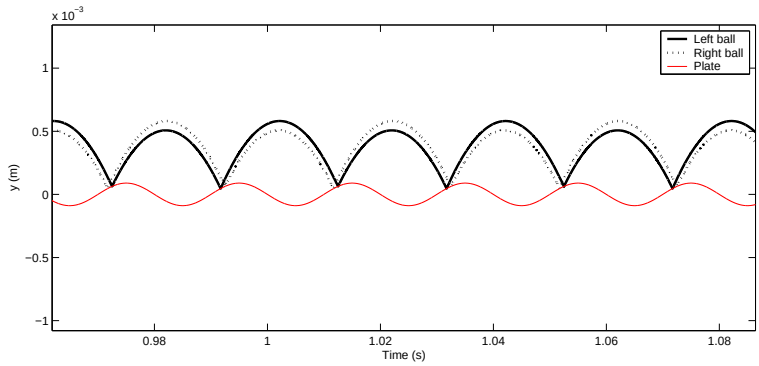

Figure 20: A zoomed picture from Figure (19).

Therefore, the ratio of the energy for the drift, jump, and flutter modes is approximately $E_d : E_j : E_f = 1 : 2 : 8$, which is consistent with the statement in [38] and the numerical observation presented in this paper.

Obviously, the formation of a persistent motion means that the energy taken by the dimer will converge to a stable energy level that is maintained by its external environment. The convergence of the energy depends on the mechanism of the exchange between energies in the dimer and the oscillated plate. This exchange is implemented through the collisions between the dimer and the plate, and the stick-slip modes. Therefore, the initial conditions of the dimer, the plate oscillation and the property of the frictional collisions will significantly influence the formation of the persistent motion.

Let us first investigate the effects from the initial energy on the modes of the persistent motions in the dimer. For a dimer with $A_r = 3.9$ under a plate oscillation with $f = 50$Hz and $\Gamma = 0.9$, the numerical simulation shows that a stable drift mode can be formed when it is released with a small initial energy. However, the increase of the initial energy will trigger a transition from a drift to a jump mode. The vertical position

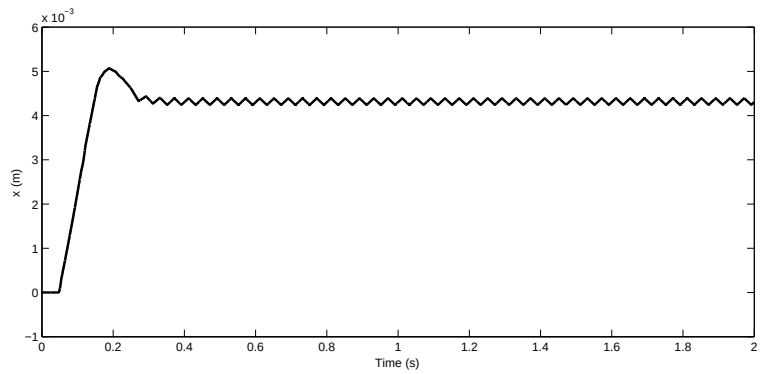

Figure 21: the horizonal position of the tip in the left (solid line) and right (dashed line) ball for dimer ($A_r = 3.9$, $f = 50$Hz, $\Gamma = 0.9$) in a jump mode generated by an initial condition of $h_0 = 10.25mm$ and $\theta_0 = 8°$. Parameters of simulations are $e_s = 0.65$, $\mu_s = 0.24$, $\mu^c = 0.12$, $\mu^i = 0.08$.

for the dimer released with the initial conditions $h = 10.25mm$ and $\theta = 8°$ is shown in Fig.19 and 20, in which a jump mode where both tips collide against the plate once every cycle appears in the dimer, and a horizonal reciprocating movement appears in the tips as shown in Fig.21.

As noted in [38], the external energy involved in the plate oscillation also plays a significant role for the formation of the persistent motion. For example, Dorbolo's experiments have shown that, for a dimer with fixed $A_r = 3.9$ and $f = 25Hz$, a stable persistent drift motion can be observed over a range of $\Gamma \in [0.5, 1.1]$, while the drift mode will spontaneously collapse to rest if $\Gamma < 0.5$, or will be unstable with respect to the transition to the higher energy jump and flutter modes and their combinations if $\Gamma > 1.1$.

Fig.22 shows the numerical results for a dimer with $A_r = 3.9$ falling on the plate with an oscillation $f = 25Hz$ and $\Gamma = 0.2$. We can find that the dimer will quickly rest on the plate for the case of the plate with a weakening vibration.

Let us fix the values of $A_r = 3.9$ and $f = 25Hz$, but increase the magnitude of the plate vibration ($\Gamma = 1.4$). Fig.23 shows the simulation results for the dimer freely dropped on the plate with initial conditions $h_0 = 0.25mm$ and $\theta_0 = 10°$. In this case, the vertical motion of the left ball seems to be harmonic with the plate oscillation, while the right ball will alternately collide against the plate with a big and a small bounces in each two adjacent cycles of the plate oscillation.

The above mode is unstable and sensitive to the initial conditions of the dimer. Let us carry out the numerical simulation by setting $h_0 = 3.25mm$ and $\theta_0 = 10°$ for the same dimer dropped on the plate with the same oscillation. Fig.24 shows that a combination of jump and flutter modes appears in the dimer motions, in which the left ball collides against the plate once during every cycle, while the right ball bounces on the plate once during every two cycles of the plate oscillation. The increases of the initial energies involved in both the left and right balls will make the two adjacent bounces at the right ball be merged, and generate a big separation between the left ball and the oscillated plate.

The formation of an ordered persistent motion is also influenced by the initial value of the tilt angle in the dimer. A new mode is triggered when the dimer is released with

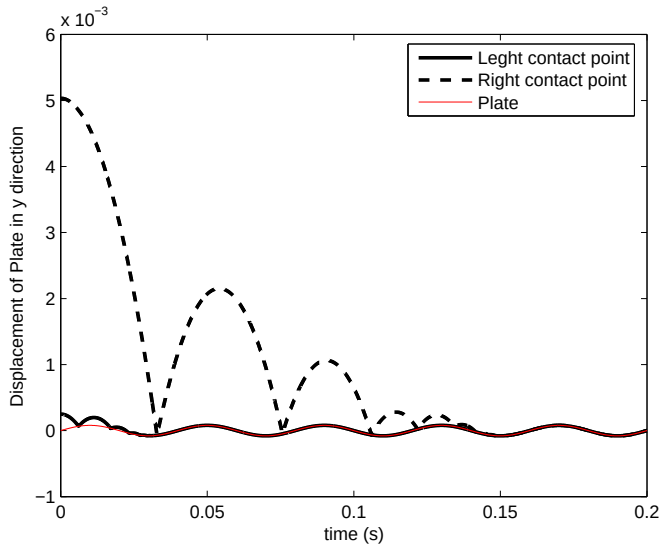

Figure 22: the horizonal position of the tip in the left (solid line) and right (dashed line) balls for dimer ($A_r = 3.9$, $f = 25$Hz, $\Gamma = 0.2$) generated by an initial condition of $h_0 = 0.25mm$ and $\theta_0 = 12°$. Parameters of simulations are $e_s = 0.65$, $\mu_s = 0.24$, $\mu^c = 0.12, \mu^i = 0.08$.

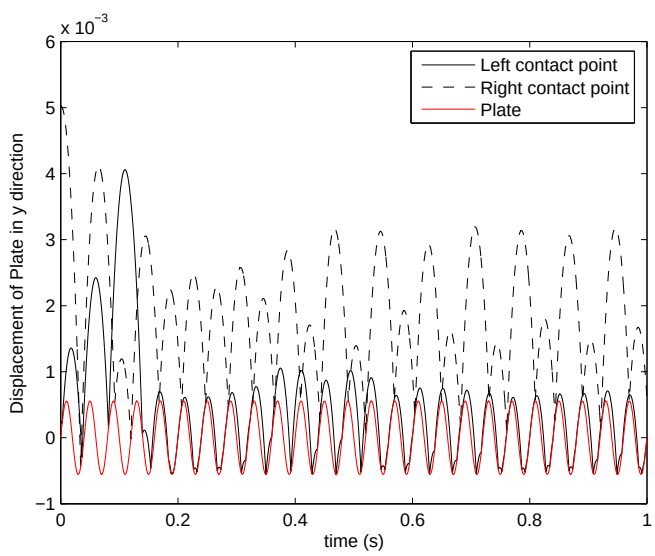

Figure 23: the horizonal position of the tip in the left (solid line) and right (dashed line) balls for dimer ($A_r = 3.9$, $f = 25$Hz, $\Gamma = 1.4$) generated by an initial condition of $h_0 = 0.25mm$ and $\theta_0 = 10°$. Parameters of simulations are $e_s = 0.65$, $\mu_s = 0.24$, $\mu^c = 0.12, \mu^i = 0.08$.

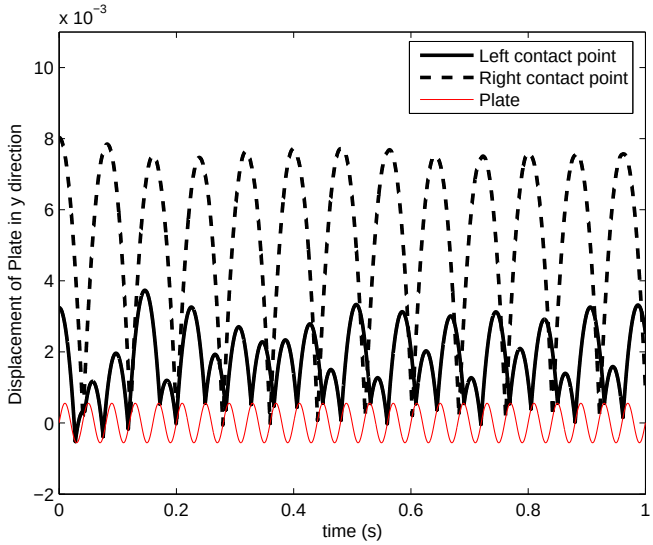

Figure 24: the horizonal position of the tip in the left (solid line) and right (dashed line) balls for dimer ($A_r = 3.9$, $f = 25$Hz, $\Gamma = 1.4$) generated by an initial condition of $h_0 = 3.25mm$ and $\theta_0 = 10°$. Parameters of simulations are $e_s = 0.65$, $\mu_s = 0.24$, $\mu^c = 0.12$, $\mu^i = 0.08$.

a small height and a small tilt angle. Fig.25 shows the results obtained by setting the initial conditions with $h_0 = 0.25mm$ and $\theta_0 = 5°$. The small initial tilt angle degrades the impact intensity at the right ball, thus makes the dimer's motion converge to a new stable status. The local picture Fig.26 (zoomed from Fig.25) shows that the dimer does not rest permanently on the plate, but leaves it with a small height during a half part of every cycle of the plate oscillation.

It is clear that the exchange between the energies involved in the dimer and the plate depends on the property of the impact between the dimer and the plate. Let us change the value of the coefficient of restitution e_s. The dimer is freely dropped from a height $h_0 = 0.25mm$ and an angle $\theta_0 = 4°$, with an oscillation $f = 50Hz$ and $\Gamma = 0.9$. The numerical simulation is carried out by setting $e_s = 0.8$ and keeping other simulation parameters with the same values as used in previous cases. Fig.27 shows the vertical positions of the tips in the dimer. Clearly, a flutter mode is generated, in which both the left and right balls hit the plate out of phase at every other period of oscillation. During the flutter mode, the tilt angle θ (see Fig.28) can vary periodically from positive to negative values.

7 The approximated formula for the mean drift speed

Let us recall the scenario of the dimer with a stable drift motion. As noted in numerical and experimental findings, the dimer in this mode seems to be driven by a periodic motion that consists of a complex structure. Furthermore, one end of the dimer hits the plate once every cycle of the plate oscillation while the other end appears to stay on the plate with forward and/or reverse slip throughout the cycle. Therefore, the

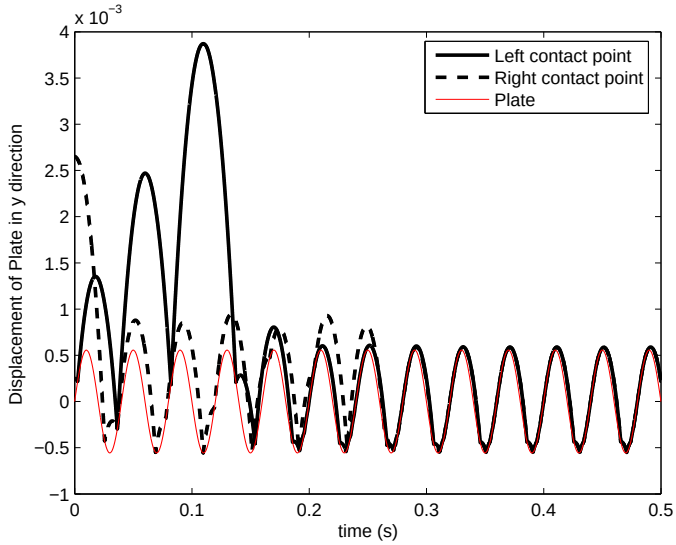

Figure 25: the horizonal position of the tip in the left (solid line) and right (dashed line) balls for dimer ($A_r = 3.9$, $f = 25$Hz, $\Gamma = 1.4$) generated by an initial condition of $h_0 = 0.25mm$ and $\theta_0 = 5°$. Parameters of simulations are $e_s = 0.65$, $\mu_s = 0.24$, $\mu^c = 0.12$, $\mu^i = 0.08$.

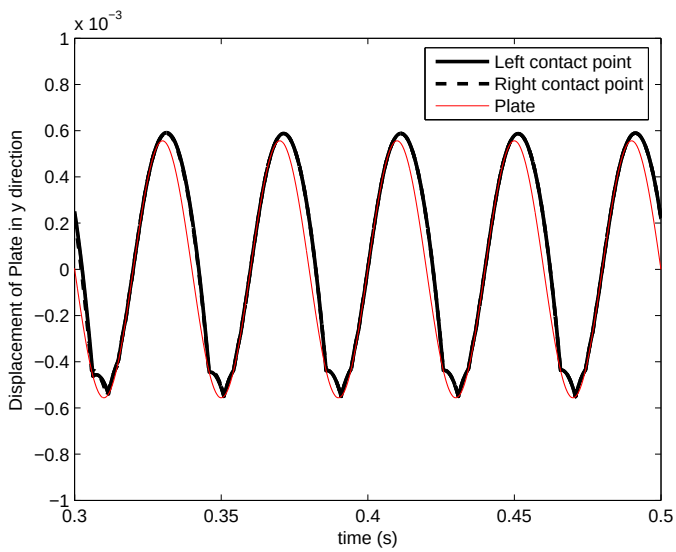

Figure 26: A local picture zoomed from Fig.25 for the horizonal position of the tip in the left (solid line) and right (the dashed line) balls for dimer ($A_r = 3.9$, $f = 25$Hz, $\Gamma = 1.4$.)

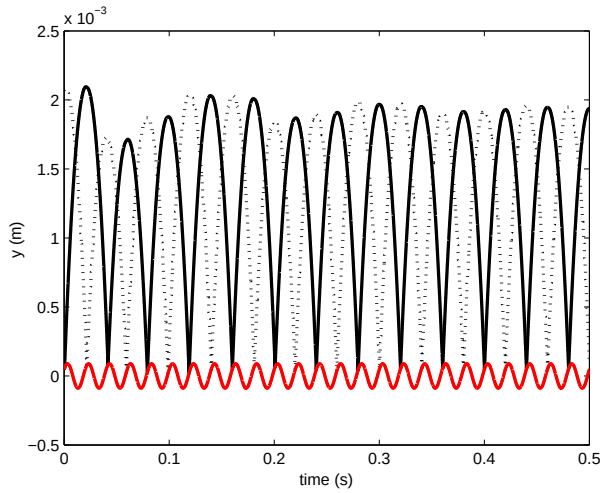

Figure 27: The vertical position of the tips in left (solid line) and right (dashed line) of the dimer ($A_r = 3.9$, $f = 50$Hz, $\Gamma = 0.9$) in a flutter mode generated by an initial condition of $h = 4.9mm$ and $\theta = 4°$. The simulation parameters are $e_s = 0.8$, $\mu_s = 0.24$, $\mu^c = 0.12$, $\mu^i = 0.08$.

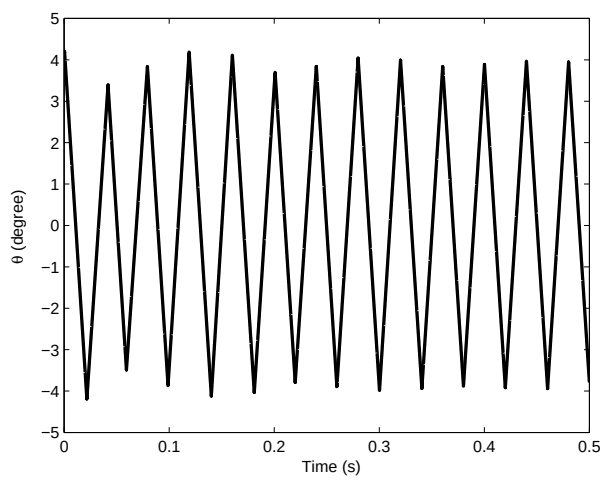

Figure 28: The angle θ as a function of time for the dimer ($A_r = 3.9$, $f = 50$Hz, $\Gamma = 0.9$) in a flutter mode. Parameters of simulations are $e_s = 0.8$, $\mu_s = 0.24$, $\mu^c = 0.12$, $\mu^i = 0.08$, $h_0 = 0.25$mm, $\theta_0 = 4$.

dimer in a drift mode can be approximately characterized by a special "unilateral single pendulum" system that satisfies the following assumptions:

- *the left ball always stays and slides on the oscillated plate during drift motion;*
- *the period of the "unilateral single pendulum" is equal to the period of the plate oscillation,* $T = 1/f$*;*

The assumption that the left ball stays on the oscillated plate corresponds to the situation of the dimer experiencing a contact phase in the drift mode. Therefore, Eq.14 and Eq.15 are just the governing equations for the "unilateral single pendulum" system, in which the contact forces at the end of the right ball are set as $(F_{n_2}, F_{\tau_2}) = (0, 0)$ since the contact at the right ball is open. According to the numerical simulation for the dimer with a drift mode, the maximal tilt angle θ is in general very small (see Fig.4 and 8). Thus the 2×2 matrices **A**, **B**, **C** and **D** in Eq.14 and 15 can be considered as constant by setting $\theta = 0$. Further simplifications can be made by ignoring the effects of the light glass rod and the inertial terms. Then, the tangential and normal accelerations of the left ball tip can be expressed as

$$\ddot{x}_{\tau_1}(t) = \frac{1}{m_b}[(\frac{1}{2} + \frac{2}{1.6 + B_r^2})F_{\tau_1}(t) - \frac{B_r}{1.6 + B_r^2}F_{n_1}(t)] \tag{125}$$

$$\ddot{x}_{n_1}(t) = \frac{1}{m_b}[-\frac{B_r}{1.6 + B_r^2}F_{\tau_1}(t) + \frac{0.8 + B_r^2}{1.6 + B_r^2}F_{n_1}(t)] - g \tag{126}$$

where $B_r = l/r$ and $A_r = 1 + 0.5B_r$.

As noted and analyzed in numerical simulations, the net motion of the dimer in the drift mode can be directed positively or negatively depending on the value of A_r. In every cycle of a positive drift motion, the tip of the left ball will first slip positively then reverse its direction. If the positive part of the integration of the horizonal speed over each cycle is larger than the one of the negative part, a net positive drift motion is generated. In the negative drift motion, the tip of the left ball only has a negative tangential velocity that appears when the frictional cone at the left end is shaken off.

Let us first investigate the case of a positive drift mode. Due to the peculiar property of Coulomb's friction, the positive drift motion should be piecewise analyzed. Let us denote $[t_s, t_1]$ and $[t_1, t_e]$ the time intervals for the positive and negative drift motions, respectively. In this case, the Coulomb's friction is $F_{\tau_1} = -\mu F_{n_1}$ and $\dot{x}_{\tau_1}(t_1) = 0$, thus during the positive slip process the horizonal speed $\dot{x}_{\tau_1}(t)$ at any time t can be obtained by integrating Eq.125 over a time interval $[t, t_1]$,

$$\dot{x}_{\tau_1}(t) = \frac{1}{2m_b(B_r^2 + 1.6)}[\mu(B_r^2 + 5.6) + 2B_r]\int_t^{t_1} F_{n_1}(s)ds \tag{127}$$

The term $\int_t^{t_1} F_{n_1}(s)ds$ is related to the normal impulse during a time interval $[t, t_1]$, and can be calculated by the analysis for the normal motion of the left ball. Using the relationship $F_{\tau_1} = -\mu F_{n_1}$ and integrating Eq.126 over a time interval $[t, t_1]$ leads to

$$\dot{x}_{n_1}(t) = \dot{x}_{n_1}(t_1) + g(t_1 - t) - \frac{1}{m_b(1.6 + B_r^2)}[B_r^2 + \mu B_r + 0.8]\int_t^{t_1} F_{n_1}(s)ds \tag{128}$$

According to the assumption that the left tip always stays on the oscillated plate, we have

$$x_{n_1}(t) = y_p(t), \quad \text{and} \quad \dot{x}_{n_1}(t) = \dot{y}_p(t) \tag{129}$$

Moreover, numerical simulations and experimental findings show that, for each cycle of the drift motion, the positive horizonal motion mostly starts when the right ball collides with the plate, before the plate oscillation reaches its positive maximal position (see Fig.3 and Fig.3(b) in [38]). Let us denote α the phase angle for the time lag between the instant of the collision starting and the one of the plate vibration with positive maximal position. The normal displacement and velocity at the tip of the left ball can be expressed as

$$\begin{aligned} x_{n_1}(t) &= y_p(t) = A\cos(\omega(t - t_s) - \alpha) \\ \dot{x}_{n_1}(t) &= \dot{y}_p(t) = -A\omega\sin(\omega(t - t_s) - \alpha) \end{aligned} \tag{130}$$

where A is the amplitude of the plate oscillation.

Let us introduce a new assumption according to the detailed observation of the numerical simulation:

- *a discontinuous transition from forward (or stick) to reverse slip at the staying end of the "unilateral single pendulum" occurs at the time when the plate vibration reaches its minimal position.*

Thus, we have $\dot{x}_{n_1}(t_1) = \dot{y}_p(t_1) = 0$ at time t_1 for the end of positive slip motion, and the impulse $\int_t^{t_1} F_{n_1}(s)ds$ can be obtained according to Eq.128

$$\int_t^{t_1} F_{n_1}(s)ds = \frac{m_b(1.6 + B_r^2)}{0.8 + B_r^2 + \mu B_r}[g(t_1 - t) + A\omega\sin(\omega(t - t_s) - \alpha)] \tag{131}$$

Since the period of the "unilateral single pendulum" is approximately equal to the one of the plate oscillation for a stable drift motion, the above assumption for a discontinuous transition from forward (or stick) to reverse slip at the staying end also means that the two parts for the positive ($\triangle t_p$) and negative ($\triangle t_n$) slip motion are divided into

$$\triangle t_p = t_1 - t_s = \frac{\pi + \alpha}{2\pi}T, \quad \triangle t_n = t_e - t_1 = \frac{\pi - \alpha}{2\pi}T \tag{132}$$

Substituting Eq.131 into (127) to obtain the horizonal speed $\dot{x}_{\tau_1}(t)$ for the tip of the left ball at time t, and integrating $\dot{x}_{\tau_1}(t)$ over the time interval $[t_s, t_1]$, the positive horizonal displacement $\langle x\rangle_p$ for each cycle of the drift motion is

$$\langle x\rangle_p = \frac{\mu(2.8 + 0.5B_r^2) + B_r}{0.8 + B_r^2 + \mu B_r}[A(1 + \cos\alpha) + 0.5g\triangle t_p^2] \tag{133}$$

Similarly, the negative displacement during the period of the reverse slip $[t_1, t_e]$ can also be obtained according to Eq.125, in which the Coulomb's friction becomes $F_{\tau_1} = \mu F_{n_1}$. Based on the assumption that $\dot{x}_{\tau_1}(t_1) = 0$, the horizonal velocity $\dot{x}_{\tau_1}(t)$ during $[t_1, t_e]$ is

$$\dot{x}_{\tau_1}(t) = \frac{1}{2m_b(B_r^2 + 1.6)}[\mu(B_r^2 + 5.6) - 2B_r]\int_{t_1}^{t} F_{n_1}(s)ds \tag{134}$$

and

$$\int_{t_1}^{t} F_{n_1}(s)ds = \frac{m_b(1.6 + B_r^2)}{B_r^2 - \mu B_r + 0.8}[g(t - t_1) - A\omega \sin(\omega(t - t_1) - \alpha)] \tag{135}$$

Then, the negative displacement $\langle x \rangle_n$ of the dimer experiencing in $[t_1, t_e]$ can be expressed as

$$\langle x \rangle_n = \frac{\mu(2.8 + 0.5B_r^2) - B_r}{0.8 + B_r^2 - \mu B_r}[A(1 + \cos\alpha) + 0.5g\triangle t_n^2] \tag{136}$$

Obviously, the net horizonal displacement during every cycle of the drift motion is the sum of $\langle x \rangle_p$ and $\langle x \rangle_n$. Let us introduce the following parameters:

$$a = \mu(2.8 + 0.5B_r^2), \quad b = B_r, \quad c = 0.8 + B_r^2, \quad d = \mu B_r, \quad \Gamma = 4\pi^2 A f^2/g \tag{137}$$

Then, the mean drift speed for the dimer in the positive drift mode is

$$\frac{\langle x \rangle_p + \langle x \rangle_n}{T} = \frac{2A}{(c^2 - d^2)T}[(1 + \cos\alpha)(ac - bd) + \frac{(\pi^2 + \alpha^2)(ac - bd) + (bc - ad)\pi\alpha}{\Gamma}] \tag{138}$$

A scaled mean drift speed is defined by

$$\kappa_{p/n} = (\langle x \rangle_p + \langle x \rangle_n) f^2 g^{-1} 10^2 \tag{139}$$

and κ_p, κ_n for the dimer in the positive and negative modes, respectively. Thus,

$$\kappa_p = \frac{50}{\pi^2(c^2 - d^2)}[(1 + \cos\alpha)(ac - bd)\Gamma + (\pi^2 + \alpha^2)(ac - bd) + (bc - ad)\pi\alpha] \tag{140}$$

If the dimer is in the negative drift mode, the positive slip at the tip of the left sphere is absent, so $\langle x \rangle_p = 0$. Keeping the assumptions used for the case of the dimer in positive drift mode, the net horizonal displacement in negative drift mode is simply equal to $\langle x \rangle_n$. Therefore, the scaled mean drift speed for the dimer in negative drift mode can be expressed as

$$\kappa_n = \frac{25(a - b)}{\pi^2(c - d)}[(1 + \cos\alpha)\Gamma + 0.5(\pi - \alpha)^2] \tag{141}$$

From Eq.140 and 141, it is clear that the scaled mean drift speed is independent of the frequency of the plate oscillation for a fixed Γ, but will be influenced by the value of the phase angle α. Fig.29 shows the scaled mean drift speed by setting $\alpha = 0$ for the parameter $\Gamma = 0.9$.

According to Eq.132, setting $\alpha = 0$ means that the positive and negative slip motions at the tip of the left ball take the same time intervals during a cycle for its drift motion. This obviously disagrees with the phenomena shown in Fig.13 (also Fig.3 in [38]) for the dimers with $A_r = 3.9$ and $A_r = 5.7$. In fact, for a dimer with a positive drift mode, the time interval $\triangle t_p$ for the positive slip motion is longer than $\triangle t_n$ related to the part of the negative slip motion. Based on the numerical observation, the phase angle α corresponds to a range $\alpha \in [\pi/10, \pi/6]$.

Fig.30 presents the scaled mean drift speed by setting $\alpha = \pi/6$ for the parameter $\Gamma = 0.9$. Clearly, for the part of the dimer with positive drift mode, the scaled mean drift speed obtained from the approximate formula is significantly improved and can

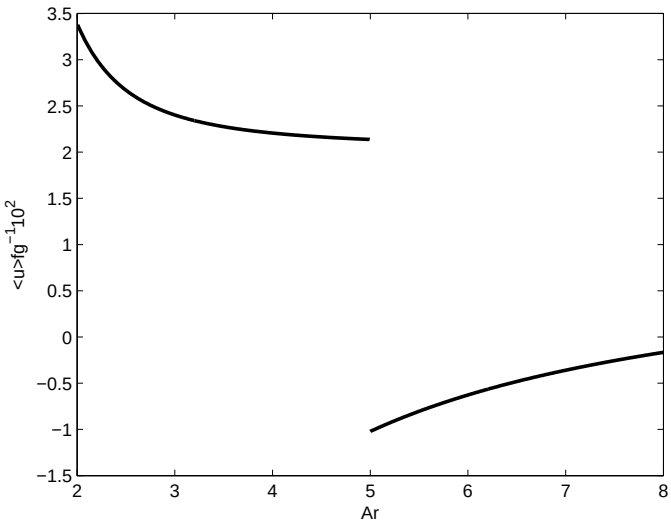

Figure 29: The scaled mean drift speed versus A_r obtained from Eq.140 and 141: $\alpha = 0$, $\Gamma = 0.9$ and $\mu = 0.12$.

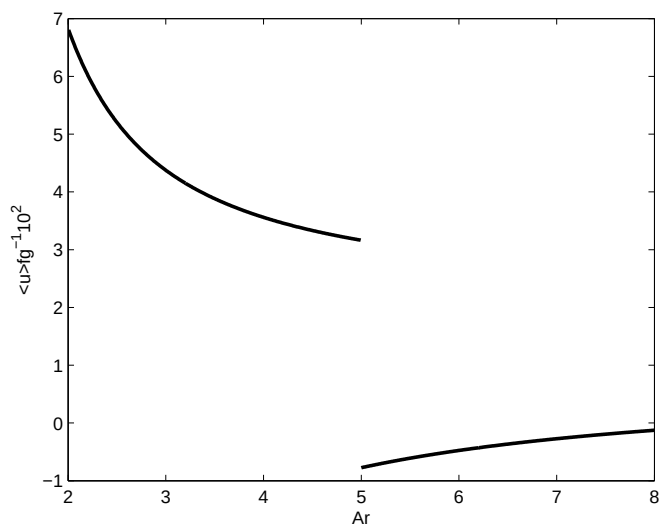

Figure 30: The scaled mean drift speed versus A_r obtained from Eq.140 and 141: $\alpha = \pi/6$, $\Gamma = 0.9$ and $\mu = 0.12$.

well coincide with the experimental findings (see Fig.4(a) [38]) and the numerical discoveries shown in Fig.15. However, in the case of the dimer with negative drift mode, a relative large deviation between them can be observed. This is because the instant for a reverse slip in the dimer with a negative drift mode is usually prior to the time t_1 for the plate oscillation reaching its minimal position, contradicting the above assumption. However, the quantitative property of the negative drift motion is still kept in the approximate formula.

8 Summary and conclusions

This paper deals with the modelling and numerical simulation of a dimer bouncing on a vibrated table, that is a nonsmooth mechanical system subject to impacts (single and double impacts) with friction. The Darboux-Keller model of multiple impacts introduced in [47] is applied and extended to the case with Coulomb friction. The variable structure dynamics is carefully described, and an event-driven numerical method is used to perform simulations. The transition rules to monitor the switches from one mode to another are established. In particular, a *correlative coefficient of friction* is introduced to analyze the complex structure of dynamics induced by the friction at contact points. The simulation results are compared to the experimental results reported in [38]. It is shown that the proposed model and numerical method allow one to recover precisely the experiments.

The mechanism of the ordered behavior exhibited in the bouncing dimer is also theoretically analyzed according to the theory proposed in this paper, which leads to a reasonable estimation for the frictional property between the dimer and the oscillated plate. Qualitative and numerical investigations indicate that each ordered persistent behavior in the dimer usually holds a quasi periodic motion that takes a complex structure but converges to a stable energy level. The pattern and formation of the stable persistent motions depend on the initial conditions and the regime of energy exchange between the system and external environment where friction and multiple shocks play a prominent effects. An attempt is made to establish the connection between the global behavior of the drift motion in the dimer and the microsize parameters of the dimer's dynamics. In terms of a simplified model, an approximate formula for the mean horizonal velocity is obtained that also coincides well with the experimental findings. These results therefore pave the way towards a reliable numerical scheme for shape matters, and may highlight the study for the collective dynamics in complex systems.

acknowledgments The support of the National Science Foundation of China (10772002) is gratefully acknowledged.

References

[1] W. Schiehlen, Multibody Sys. Dyn. 1: 149, (1997).

[2] F. Pfeiffer, Ch. Glocker, Multibody Dynamics with Unilateral Contacts. Wiley Series in Nonlinear Science, (1996).

[3] B. Brogliato. Nonsmooth Mechanics, 2nd edition. Springer, London, (1999).

[4] D.Stewart, SIAM Rev. 42(1), 3C39 (2000).

[5] I. S. Aranson, Lev S. Tsimring, Reviews of Modern Physics,78,641-692 (2006).

[6] M.J. Coleman, A Ruina, Phys. Rev. Lett. 80: 3568, (1998).

[7] M. V. Hecke, Science, 317, 49-50 (2007).

[8] V. Narayan, S. Ramaswamy, N. Menon, Science, 317, 105-108 (2007).

[9] C. Goldenberg, and I. Goldhirsch, 2005, Nature 435, 188.

[10] B. Brogliato, A.A. ten Dam, L. Paoli, F. Génot, M. Abadie, Appl. Mech. Rev. ASME, 55(2):107, (2002).

[11] C. Liu, Z. Zhao, B.Chen, Nonlinear Dyn. 49:217, (2007).

[12] Z. Zhao, C.Liu, W. Ma, B. Chen, J. Appl. Mech. 75, 041006, (2008).

[13] Z. Zhao, C.Liu, B.Chen, Multibody Syst. Dyn. 19:323, (2008).

[14] A.P. Ivanov, J. Appl. Math. Mech. 67(2), 185 (2003).

[15] W.J. Stronge, Impact Mechanics, Cambridge University Press, (2000).

[16] J.B. Keller, ASME J. Appl. Mech. 53:1 (1986).

[17] C. Liu, Z. Zhao, and B. Brogliato, INRIA Research report, 2008 (unpublished), http://hal.inria.fr

[18] V. Acary, B. Brogliato. Numerical Methods for Nonsmooth Dynamical Systems. Applications in Mechanics and Electronics. Springer, LNACM 35, Heidelberg, (2008).

[19] S. Sen, J. Hong, J. Bang, E. Avalosa, R. Doneyd, Phy. Rep. 462, 21-66, (2008)

[20] V. F. Nesterenko, J. Appl. Mech. Tech. Phys. (USSR) 5, 733C743, (1983).

[21] E. Falcon, C. Laroche, S. Fauve, and C. Coste, Eur. Phys. J. B, 5, 111-131, (1998).

[22] V. F. Nesterenko, C. Daraio, E. B. Herbold, and S. Jin, Phys. Rev. Lett. 95, 158702 (2005).

[23] S. Job, F. Melo, S. Sen, and A. Sokolow, Phys. Rev. Lett. 94, 017802 (2005).

[24] L. Vergara, Phys. Rev. Lett. 94, 108002 (2005).

[25] T. S. Majmudar, M. Sperl, S. Luding, and R. P.Behringer, Phys. Rev. Lett. 98, 058001 (2007).

[26] E.J. Hinch and S. Saint-Jean, Proc. R. Soc. London, Ser. A 455, 3201 (1999).

[27] J. Hong, Phys. Rev. Lett. 94, 108001 (2005).

[28] A. Rosas and K. Lindenberg, Phys. Rev. E 68, 041304 (2003).

[29] M. Wei, C. Liu, B. Chen, L. Huang, Phys. Rev. E 74, 046602 (2006).

[30] Z. Zhao, C.Liu, B. Brogliato, Phys. Rev. E 78, 031307 (2008).

[31] P.Wang, J. Xia, Y. Li, and C.Liu, Phys. Rev. E, 76, 041305 (2007).

[32] J. Crassous, D. Beladjine, and A. Valance, Phy. Rev. Lett. 99, 248001 (2007).

[33] I. S. Aranson, D. Volfson, and L. S. Tsimring, Phys. Rev. E, 75, 051301 (2007).

[34] D. Volfson, A. Kudrolli, and L. S. Tsimring, Phys. Rev. E, 74, 061309 (2006).

[35] I. S. Aranson, L. S. Tsimring, Phys. Rev. E, 67, 021305 (2003).

[36] H. S. Wright, M. R. Swift, and P. J. King, Phys. Rev. E 70, 051312 (2004) (2006).

[37] M. Ramaioli, L. Pournin, and Th. M. Liebling, Phys. Rev. E 76, 021304 (2007).

[38] S. Dorbolo, D. Volfson, L. Tsimring, and A. Kudrolli, Phys. Rev. Lett. 95, 044101 (2005).

[39] S. McNamara, E. Falcon,Phys. Rev. E 71, 031302 (2005).

[40] S. McNamara, E. Falcon, Powder Technology 182,232, (2008).

[41] M.H. Sadd, Q. Tai, A. Shukla, Int. J. Non-Linear Mechanics, vol.28, no 2, pp.251-265, (1993).

[42] S. Luding, Granular Matter 10(4), (2008).

[43] S. Peng, P. Kraus, V.Kumar, P.Dupont, ASME J. Appl. Mech. 68, 118 (2001).

[44] Ch. Glocker, Set-Valued Force Laws. Springer, LNAM 1, Heidelberg (2001).

[45] Z. Zhen, C.Liu, Multibody Syst Dyn 18: 511 (2007).

[46] Z. Zhen, C.Liu, B.Chen, Sci. in China(G), 49:102, (2006).

[47] C. Liu, Z. Zhao, B. Brogliato, Proc. Roy. Soc. A, 464, 3193-3211 (2008).

[48] C. Liu, Z. Zhao, B. Brogliato, Proc. Roy. Soc. A, (2008) (published online, doi/0.1098 /rspa.2008.0079).

[49] G.Darboux, Bull. Sci. Math. Astron. 4, 126 (1880).

[50] W.Yao, B. Chen, C. Liu, Int. J. Imp. Eng. 31 255, (2005).

[51] A.Kudrolli, G.Lumay, D.Volfson, and L. Tsimring, Phys. Rev. Lett. 100, 058001 (2008).

[52] P. Painlevé, C. R. Hebd. Seances Acad. Sci., 121: 112, (1895).

[53] F. Génot, B. Brogliato, Eur. J. Mech. A/Solids, 18:653, (1999).

[54] V. Bhatt, J. Koechling, Trans. ASME J. Appl. Mech. 62: 740 (1995).

[55] V. Bhatt, Trans. ASME J. Appl. Mech. 62:893, (1995).

[56] W.J. Stronge, Trans. ASME J. Appl. Mech. 61:605 (1994).

[57] E. Falcon, C. Laroche, S. Fauve, and C. Coste, Eur. Phys. J. B 3: 45 (1998).

[58] S. McNamara, W.R. Young, Phys. Rev. E 50, R28 (1994).

[59] P. Constantin, E. Grossman, M. Mungan, Physica D 83, 409 (1995).

[60] K. L. Johnson. Contact Mechanics. Cambridge Univ. Press, Cambridge, (1989).

[61] H. Lankarani and P. Nikravesh, Nonlinear Dynamics, vol.5, 193-207, (1994).

Contents

1 Introduction **4**

2 The dynamics of a bouncing dimer **7**

3 The topology of the contact states **9**
3.1 The complementary condition in the normal direction 10
3.2 Coulomb's friction 10
3.3 Transition between various system states 11
3.4 The singularity in contact phases 14

4 Impact dynamics with friction **16**
4.1 Impulsive differential equations 16
4.2 The normal and tangential constraints for impacts 17
4.3 The distributing law for multiple impacts 18
4.4 The topology of impacts with friction 19
4.4.1 A single impact with friction 19
4.4.2 Double impacts with friction 21
4.5 The singularity in double impacts and the inelastic collapse 23

5 Qualitative analysis for the drift motion in the bouncing dimer **25**
5.1 Experimental phenomenon in the dimer 25
5.2 The correlative coefficient of friction 25
5.3 Estimation of the coefficient of friction 27
5.4 Qualitative analysis of the drift mode 28

6 comparison between numerical and experimental results **31**
6.1 The preliminary numerical results 31
6.2 Numerical results obtained by modifying the slip coefficient of friction 41
6.3 Other stable persistent motion shown in the dimer 47

7 The approximated formula for the mean drift speed **51**

8 Summary and conclusions **58**

Centre de recherche INRIA Grenoble – Rhône-Alpes
655, avenue de l'Europe - 38334 Montbonnot Saint-Ismier (France)

Centre de recherche INRIA Bordeaux – Sud Ouest : Domaine Universitaire - 351, cours de la Libération - 33405 Talence Cedex
Centre de recherche INRIA Lille – Nord Europe : Parc Scientifique de la Haute Borne - 40, avenue Halley - 59650 Villeneuve d'Ascq
Centre de recherche INRIA Nancy – Grand Est : LORIA, Technopôle de Nancy-Brabois - Campus scientifique
615, rue du Jardin Botanique - BP 101 - 54602 Villers-lès-Nancy Cedex
Centre de recherche INRIA Paris – Rocquencourt : Domaine de Voluceau - Rocquencourt - BP 105 - 78153 Le Chesnay Cedex
Centre de recherche INRIA Rennes – Bretagne Atlantique : IRISA, Campus universitaire de Beaulieu - 35042 Rennes Cedex
Centre de recherche INRIA Saclay – Île-de-France : Parc Orsay Université - ZAC des Vignes : 4, rue Jacques Monod - 91893 Orsay Cedex
Centre de recherche INRIA Sophia Antipolis – Méditerranée : 2004, route des Lucioles - BP 93 - 06902 Sophia Antipolis Cedex

Éditeur
INRIA - Domaine de Voluceau - Rocquencourt, BP 105 - 78153 Le Chesnay Cedex (France)
http://www.inria.fr
ISSN 0249-6399